AGU PUBLICATIONS

Journal of Advances in Modeling Earth Systems

RESEARCH ARTICLE

10.1002/2016MS000802

Organization of tropical convection in low vertical wind shears: Role of updraft entrainment

Adrian M. Tompkins[1] and **Addisu G. Semie**[1,2]

[1]Earth System Physics, Abdus Salam International Centre for Theoretical Physics, Trieste, Italy, [2]Now at: Laboratoire de Météorologie Dynamique, Paris, France

Key Points:
- Updraft entrainment a critical process for spontaneous organization of deep convection
- With O(km) horizontal grid sizes, updraft entrainment represented by subgrid turbulence schemes, approaches vary by orders of magnitude
- Critical role of model assumptions highlights need for simulation ensembles and community organization model intercomparison project

Correspondence to:
A. Tompkins,
tompkins@ictp.it

Citation:
Tompkins, A. M., and A. G. Semie (2017), Organization of tropical convection in low vertical wind shears: Role of updraft entrainment, *J. Adv. Model. Earth Syst.*, *9*, 1046–1068, doi:10.1002/2016MS000802.

Received 6 SEP 2016
Accepted 5 APR 2017
Accepted article online 14 APR 2017
Published online 5 MAY 2017

Abstract Radiative-convective equilibrium simulations with a 2 km horizontal resolution are conducted to investigate the impact on convective organization of different parameterizations for horizontal and vertical subgrid turbulence mixing. Three standard approaches for representing horizontal diffusion produce starkly differing mixing rates, particularly for the entrainment mixing into updrafts, which differ by more than an order of magnitude between the schemes. The simulations demonstrate that the horizontal subgrid mixing of water vapor is key, with high mixing rates a necessary condition for organization of convection to occur, since entrainment of dry air into updrafts suppresses convection. It is argued that diabatic budgets, while demonstrating the role of spatially heterogeneous radiative heating rates in driving organization, can overlook the role of physical processes such as updraft entrainment. These results may partially explain previous studies that showed that organization is more likely to occur at coarser resolutions, when entrainment is solely represented by subgrid-scale turbulence schemes, highlighting the need for benchmark simulations of higher horizontal resolution. The recommendation is for the use of larger ensembles to ensure robustness of conclusions to subgrid-scale parameterization assumptions when numerically investigating convective organization, possibly through a coordinated community model intercomparison effort.

Plain Language Summary Thunderstorms dry out the atmosphere since they produce rainfall. However, their efficiency at drying the atmosphere depends on how they are arranged; take a set of thunderstorms and sprinkle them randomly over the tropics and the troposphere will remain quite moist, but take that same number of thunderstorms and place them all close together in a "cluster" and the atmosphere will be much drier. Previous work has indicated that thunderstorms might start to cluster more as temperatures increase, thus drying the atmosphere and letting more infrared radiation escape to space as a result - acting as a strong negative feedback on climate, the so-called iris effect. We investigate the clustering mechanisms using 2km grid resolution simulations, which show that strong turbulent mixing of air between thunderstorms and their surrounding is crucial for organization to occur. However, with grid cells of 2 km this mixing is not modelled explicitly but instead represented by simple model approximations, which are hugely uncertain. We show three commonly used schemes differ by over an order of magnitude. Thus we recommend that further investigation into the climate iris feedback be conducted in a coordinated community model intercomparison effort to allow model uncertainty to be robustly accounted for.

1. Introduction

Around 30 years ago, computing resources reached levels adequate to integrate two-dimensional and three-dimensional models with kilometer-scale grid sizes for periods of several weeks required to simulate radiative-convective equilibrium states [*Held et al*., 1993; *Tompkins and Craig*, 1998a; *Bretherton et al*., 2005]. Despite homogeneous initial conditions, convection was found to undergo strong spontaneous organization, with deep convection restricted to moist areas that were surrounded by dry convection-free regions. The organization leads to a drier mean atmosphere and increased outgoing long-wave radiation (OLR) [*Bretherton et al*., 2005; *Tobin et al*., 2012; *Wing and Emanuel*, 2013]. *Emanuel et al*. [2014] have recently suggested that organization may only occur above a threshold sea surface temperature (SST), posing the intriguing prospect of a potential negative climate feedback that may be missing from global climate models [*Mauritsen and Stevens*, 2015]. The reversal of the correlation between the top of atmosphere (TOA) OLR

© 2017. The Authors.
This is an open access article under the terms of the Creative Commons Attribution-NonCommercial-NoDerivs License, which permits use and distribution in any medium, provided the original work is properly cited, the use is non-commercial and no modifications or adaptations are made.

and SST anomalies between the west Pacific warm pool area and the central Pacific hints at this mechanism [*Trenberth et al*., 2015]. An understanding of the factors driving convective organization is thus key.

Heterogeneous radiative heating rates can impact atmospheric circulations [*Gray and Jacobson*, 1977; *Slingo and Slingo*, 1988; *Randall et al*., 1989] and a key process for convective organization involves feedback with radiation. Convective organization quickly broke up when radiative heating rates were horizontally homogenized in *Tompkins and Craig* [1998a]. Since then, a number of papers have investigated this in further detail, with the feedback variously attributed to the radiative impact of high clouds [*Stephens et al*., 2008] and low clouds [*Muller and Held*, 2012]. Both the long-wave and short-wave radiative impacts of the heterogeneous water vapor field can also drive convergence into moist regions [*Wing and Emanuel*, 2013; *Emanuel et al*., 2014; *Sessions et al*., 2016]. *Mapes and Zuidema* [1996] document the changes in the vertical stability that can result from dry layers.

Water vapor not only acts through its influence on the radiative heating; it also has a direct thermodynamical role in regulating convection [*Tompkins*, 2001a, 2001b; *Grabowski and Moncrieff*, 2004]. Dry boundary layers will inhibit convection due to their impact on convective available potential energy (CAPE) and convective inhibition (CIN), but organization also operates partly through entrainment whereby dry midtropospheres increase evaporative cooling of updrafts, reducing updraft buoyancy [*Derbyshire et al*., 2004]. *Sherwood et al*. [2010] emphasizes the precursor role of humidity for convection, while identifying an uncertain role of convective updraft entrainment. *Johnson and Lin* [1997], *Sherwood* [1999], *Bretherton et al*. [2004], and *Holloway and Neelin* [2009, 2010] demonstrate the positive relationship between atmospheric water vapor and convective activity, with increasing humidity noted as a convective precursor in some of these studies. *Tompkins* [2001a] noted a larger impact of perturbations in the 900–700 hPa layer since downdrafts immediately transported the dry anomaly to the boundary layer, effectively suppressing deep convection, while perturbations above 700 hPa merely reduced the intensity of convection through the entrainment mechanism. *Craig and Mack* [2013] developed an idealized model of upscale organization cascade resulting from the water vapor feedback. Recent investigations with cloud-resolving models have confirmed the important role of water vapor [*Holloway and Woolnough*, 2016]. *Sherwood et al*. [2010] reviews the research on water vapor feedbacks with convection and notes that the relationship can be complex. For example, in situations of higher wind shear, dry layers can enhance the probability of mesoscale squall-line formation through precipitation evaporation driving stronger downdrafts [*Roca et al*., 2005].

The maintenance of the dry anomalies is due to low horizontal mixing time scales on the mesoscale [*Pierrehumbert and Yang*, 1993; *Yang and Pierrehumbert*, 1994; *Zhang*, 2005], although it is likely enhanced in the idealized CRM setup since the periodic boundary conditions imply an absence of eddies near the domain scale, seen in the flattening of the power spectra at the largest scales [*Bretherton and Khairoutdinov*, 2015]. The exact role of water vapor entrainment on organization is far from clear though. While *Tompkins* [2001a] and *Grabowski and Moncrieff* [2004] argued for its importance (using simulations with marginally convection-resolving resolutions, a caveat that will be returned to in the discussion), *Emanuel et al*. [2014] downplayed this role when introducing a simple model for radiative-convective instabilities that omitted an explicit treatment of entrainment suppression of convection.

In summary, cloud-resolving models with grid sizes of O(1 km) have revealed many of the potential feedback processes that may lead to, or enhance, convective organization. It should be recalled however, that these studies are often idealized and involve computational compromises, as recently discussed in *Mapes* [2016]. The computational requirements of RCE experiments that require more than 40 days of integration still largely prohibit horizontal resolutions finer than 1 km. Simulations such as *Tompkins* [2001c], *Bryan et al*. [2003], and *Khairoutdinov et al*. [2009] that use resolutions less than 350 m were restricted to 1 or 2 days. If water vapor entrainment is a factor for either the establishment and/or the amplification of convective organization, it raises the issue that the organization strength in CRMs model using grid sizes of O(1 km) or larger is likely to be sensitive to the model resolution and simulation framework in terms of the choice of subgrid-scale diffusion and mixing.

At 1 km, the model grid size is comparable to the scale of the convective updrafts themselves and simulated convective updrafts will consist of one, or at most, a handful of model grid points. A more accurate alternative nomenclature for these models is therefore "convection permitting," to emphasize the fact that the resolutions employed are inadequate to truly resolve the intricacies of the subcloud scale structure,

seen in aircraft observations [e.g., *Warner and Newnham*, 1952; *Warner*, 1955]. The representation of convection in such models resembles far more the top-hat, ensemble plumes of mass-flux parameterization schemes of *Arakawa and Shubert* [1974] and *Tiedtke* [1989] than actual turbulent convection. Entrainment into the updraft cores is represented predominantly by the subgrid-scale mixing schemes and (implicit or explicit) numerical diffusion, and at these resolutions entrained air is mixed homogeneously into the core.

The impacts of the choice of subgrid-scale mixing parameterization scheme have been examined for short-term simulations of squall lines and other convective phenomena [*Takemi and Rotunno*, 2003; *Bryan*, 2005; *Knievel et al*., 2007]. *Takemi and Rotunno* [2003] stressed the importance of identifying an optimum subgrid-scale eddy mixing constant for simulations of squall lines. Two studies have examined the impact of the choice of subgrid-scale horizontal mixing scheme on realistic situations, and concluded that 3-D turbulence schemes that represented greater lateral mixing resulted in more cores with lower updraft velocities [*Machado and Chaboureau*, 2015; *Hanley et al*., 2015]. However, the impact of the subgrid-scale mixing approach has received limited attention for simulations of RCE. *Pauluis and Garner* [2006] and *Muller and Held* [2012] did investigate the sensitivity of organization to the model resolution employed, with *Muller and Held* [2012] stating the need to employ horizontal grid sizes coarser than 2 km for organization to occur, which may be attributable to the relative contributions of explicit and parameterized updraft entrainment as the resolution changes.

The aim of this paper is therefore to investigate the impact of the subgrid-scale mixing schemes on the degree of convective organization in the idealized framework of RCE over homogeneous surface conditions. A commonly used community model is employed that has a wide range of subgrid-scale parameterization approaches available. A set of long-term convection permitting simulations are performed, each with a choice of subgrid-scale schemes combinations that are recommended for use by the model designers. It will be demonstrated that the strength of the entrainment into convection is crucial to the occurrence of organized convection.

2. Materials and Methods

2.1. Model

The model used for the simulations is the nonhydrostatic WRF model [*Skamarock et al*., 2008], version 3.5.1. The fifth-order advection scheme is employed for both momentum and scalar horizontal fields [*Skamarock et al*., 2008] and the microphysics is parameterized using the Purdue Lin scheme that includes six classes of hydrometers (water vapor, cloud water, rain, cloud ice, snow, and graupel) [*Lin et al*., 1983]. The radiative transfer scheme RRTMG calculates short-wave $(RRTMG_SW)$ [*Mlawer and Clough*, 1997] and long-wave $(RRTMG_LW)$ [*Mlawer et al*., 1997; *Mlawer and Clough*, 1997] fluxes and heating/cooling rates efficiently and accurately using the correlated *k* approach. Gravity waves are damped at the domain top using Rayleigh damping to prevent unphysical wave reflection off the domain upper boundary [*Skamarock et al*., 2008].

The simulations conducted use a range of options for representing horizontal and vertical subgrid-scale mixing. The task of each mixing scheme is to specify an eddy diffusion coefficient *k* that relates the subgrid-scale flux of the mixed quantity to its resolved gradient. There are a number of options in WRF to calculate *k* using first order or 1.5 order closures. In each scheme outlined below, the WRF default minimum background mixing coefficient of 4 $m^2\ s^{-1}$ is applied. Only a brief overview is given of each scheme; for full details the reader is referred to section 4.2 of *Skamarock et al*. [2008].

2.1.1. 2-D Smagorinsky Scheme

One widely used method to calculate the eddy diffusion coefficient is the first-order closure of *Smagorinsky* [1963]. The 2-D version of this scheme only treats subgrid-scale turbulent kinetic energy generation by the shear of horizontal winds and must be supplemented with an additional scheme to represent vertical mixing. The horizontal eddy diffusion coefficient k_h is parameterized according to

$$k_h = C_s^2 l_h^2 \left[0.25(D_{11} - D_{22})^2 + \overline{D_{12}^2}^{xy} \right]^{\frac{1}{2}}, \tag{1}$$

where the first and second terms in the brackets represent the tension and shear strain deformation, respectively (see equations (4.22)–(4.24) of *Smagorinsky* [1963]). Here C_s is a constant representing the transportation efficiency of eddies, set to 0.25 in this scheme, l_h is the horizontal eddy mixing length scale,

related to the horizontal grid size as $l_h=(\Delta x\Delta y)^{\frac{1}{2}}$. D represents the wind deformation: $D_{11}=2\frac{du}{dx}$, $D_{22}=2\frac{dv}{dy}$, $D_{12}=\frac{du}{dy}+\frac{dv}{dx}$. D_{12} is averaged over x and y grid points. For scalar mixing k_h is divided by the Prandtl number (Pr).

2.1.2. 3-D Smagorinsky Scheme

The 3-D Smagorinsky scheme specifies k using both the full 3-D wind shear and static stability. As it represents vertical mixing it can be used with or without a PBL scheme. It calculates both the horizontal and vertical mixing as:

$$k_{h,v}=C_s^2 l_{h,v}^2 \max\left[0,\left(D^2-\frac{N^2}{P_r}\right)^{\frac{1}{2}}\right], \tag{2}$$

where N is the Brunt-Vaisala frequency and $D^2=\frac{1}{2}[D_{11}^2+D_{22}^2+D_{33}^2]+(\overline{D_{12}}^{xy})^2+(\overline{D_{13}}^{x\eta})^2+(\overline{D_{23}}^{y\eta})^2$, where $D_{33}=2\frac{dw}{dz}$, $D_{13}=\frac{dw}{dx}$, $D_{23}=\frac{dw}{dy}$. D_{13} and D_{23} are averaged over x and η and y and η grid points, respectively. Note that the 3-D scheme accounts for shear strain only and does not simplify to the 2-D scheme if restricted to two dimensions.

In these experiments, turbulence is thus not assumed to be isotropic since $\Delta z \ll \Delta x, y$. In this case the vertical length scale l_v is set equal to the vertical resolution, and l_h is identical to the definition used in the 2-D scheme, thus the vertical and horizontal mixing lengths differ by approximately an order of magnitude.

2.1.3. Turbulent Kinetic Energy Scheme

A 1.5 order turbulence kinetic energy ($e=\frac{1}{2}(u'^2+v'^2+w'^2)$) scheme is alternatively available, referred to as the TKE scheme. Like the 3-D Smagorinsky scheme, the TKE closure method can represent both horizontal and vertical subgrid-scale mixing, in the boundary layer and free troposphere. The standard prognostic equation for the evolution of e includes shear production, transport, buoyancy, and dissipation terms [e.g., *Stull*, 1988]. Thus, similar to the 3-D Smagorinsky scheme the full 3-D wind shear vector contributes to mixing in addition to the vertical stability. With e known at each time step, the formulation for the eddy coefficient is:

$$k_{h,v}=C_s e^{\frac{1}{2}} l_{h,v}, \tag{3}$$

where C_s is set to a default value of 0.15 in this scheme. In the TKE scheme, the horizontal eddy mixing length scale l_h is identical to that in the 3-D Smagorinsky scheme in the anisotropic case.

If a constant dissipation time scale were used, and local equilibrium assumed, it would be possible to write the TKE in terms of the wind shear, stability and dissipation time scale and insert this into equation (3) to derive a diagnostic Smagorinsky-type closure. However, in the TKE scheme, the dissipation term is set to

$$\left(1.9C_k+\frac{(0.93-1.9C_k)l}{L}\right)\frac{e^{\frac{3}{2}}}{l}, \tag{4}$$

where $L=(\Delta x\Delta y\Delta z)^{\frac{1}{3}}$ and $l=\min(L,0.76\sqrt{e}/N)$, and thus the derivation of a diagnostic scheme is not straightforward. It is emphasized that the 3-D Smagorinsky scheme in WRF is not the diagnostic equivalent of the TKE scheme and thus the domain and time mean mixing of the two schemes will not be the same.

2.1.4. Planetary Boundary Layer Scheme

Deep convection initiates in the boundary layer in RCE-type simulations and it is important to have a good representation of the well mixed layer. To facilitate this, some simulations employ the Yonsei University (YSU) Planetary boundary layer (PBL) scheme to represent the vertical subgrid-scale fluxes of the thermodynamic and dynamical quantities [*Hong et al*., 2006]. The YSU PBL scheme has an explicit treatment of the entrainment layer at the PBL top and represents nonlocal mixture using the counter gradient flux terms in the boundary layer. It should be noted that when the PBL scheme is engaged in the WRF model, it represents all vertical mixing throughout the troposphere for consistency, and is not restricted to the boundary layer. To accomplish this, above the diagnosed mixed layer top, the scheme reverts to a standard local diffusion approach to account for vertical mixing using a mixing length related to the grid resolution [*Hong et al*., 2006]. *Hu et al*. [2010] evaluated the scheme against two alternative approaches and found it one of the better performing schemes in terms of the boundary layer representation.

2.1.5. Sixth-Order Noise Filter

An optional explicit sixth-order spatial filter can be applied to locally enhance horizontal diffusion and prevent grid-scale noise and sharp gradients in dynamic and thermodynamical fields [*Xue*, 1999]. *Bryan* [2005] and *Knievel et al*. [2007] report the impact of using this scheme. The scheme can be used with or without enforcing monotonicity to prevent up-gradient transport. In the case of monotonic flux limiter, the diffusive fluxes are simply set to zero if up-gradient diffusion is diagnosed between two cells [see *Xue*, 1999, for details]. Test simulations without the sixth-order diffusion scheme revealed the presence of spurious noise and thus all simulations use the sixth-order noise filter without the imposition of monotonicity. We note that the results were sensitive to the imposition of monotonicity which effectively enhanced mixing at convective grid cells.

2.2. Simulation Setup

The domain size is 500 by 500 km with a sea surface of 301.5 K imposed as a fixed lower boundary condition and periodic lateral boundary conditions. An equatorial location is assumed and the Coriolis effect is thus ignored. The diurnal cycle is included in the simulations, and while flux quantities are accumulated, instantaneous snapshots of 3-D fields are saved at the model simulated midnight. The domain size is similar to that used by *Bretherton et al*. [2005]. *Muller and Held* [2012] found self-aggregation required domain sizes larger than 200 km although *Tompkins and Craig* [1998a] documented strong aggregation even with 100 km length 3-D domains, indicating a strong dependence of this threshold on the model configuration. *Wing and Cronin* [2016] recently introduced a theory for the spacing between convective clustered in organized states based on the boundary layer recovery that would suggest a single convective cluster is expected if convective organizes in a domain of this size. A sensitivity test of the control model integration was conducted with a larger domain of 1000 km by 500 km, and found to give similar convective organization statistics to the control configuration.

All CRM simulations use a 2 km horizontal spacing (as used by *Tompkins and Craig* [1998a], *Bretherton et al*. [2005], and *Muller and Held* [2012]) and no convective parameterization scheme is used. A stretched vertical grid divides the atmosphere up into 62 layers to ensure microphysical processes such as ice melting are well resolved [*Tompkins and Emanuel*, 2000]. The lowest model level is set to 39 m with grid spacing of only 50 m in the boundary layer, then the spacing stretches to 100 m, 200 m, 500 m, and 1 km at 5 km, 15 km, and 25 km, respectively. The domain mean horizontal wind is constrained by relaxing the winds toward zero with a time scale of $\tau =$ one hour by adding tendency terms:

$$\frac{du}{dt} = \frac{-\overline{u}}{\tau}, \frac{dv}{dt} = \frac{-\overline{v}}{\tau}, \tag{5}$$

where the overbar represents the domain mean value. This prevents the development of wind shear during the simulation, as observed in previous simulations [*Held et al*., 1993; *Tompkins and Craig*, 1998a; *Tompkins*, 2000]. The results are insensitive to the chosen time scale if it is shorter than the multiday time scale over which the spontaneous wind shear but does not impact the nature of convective or subdomain circulations.

The main experiment examines the impact of the subgrid-scale mixing scheme on the convective organization and consists of four simulations lasting 70 days. Each simulation uses a distinct combination of subgrid-scale eddy diffusion schemes, as summarized in Table 1. It is emphasized that each simulation uses a configuration recommended in the WRF user guide, and thus is likely to be regularly employed by users of the model. The first simulation (smag3dpbl) uses the 3-D Smagorinsky mixing for horizontal transport, while the YSU PBL scheme handles all subgrid-scale vertical transport. The simulation smag3d switches off the YSU scheme, and thus the 3-D Smagorinsky scheme is responsible for both horizontal and vertical transport. The difference between these two simulations is thus only in the representation of vertical mixing. The 2-D Smagorinsky scheme with YSU PBL scheme is used in the smag2dpbl simulation. Comparison of smag2dpbl and smag3dpbl will thus reveal the impact of including the full 3-D shear tensor and buoyancy in the calculation of horizontal mixing. The TKE 1.5 order closure scheme is instead employed for the final simulation, tke3dpbl, which also uses the YSU PBL scheme. The eddy mixing coefficient C_s is set to its default value of 0.15 for the TKE simulation.

Table 1. Overview of the Simulations and Their Mixing Options in the Main Experiment, Which Are Supplemented by Shorter Sensitivity Simulation Ensembles

Simulation	Horizontal Mixing	Vertical Mixing
smag3dpbl	3-D Smagorinsky	YSU PBL
smag3d	3-D Smagorinsky	3-D Smagorinsky
smag2dpbl	2-D Smagorinsky	YSU PBL
tke3dpbl	TKE ($C_s = 0.15$)	YSU PBL
Sensitivity experiments		
TKE eddy strength	TKE scheme with C_s set to 0.2, 0.3, 0.4, 0.5, or 0.6	YSU PBL
TQ-smag3dpbl	3-D Smagorinsky applied only to temperature and humidity fields	YSU PBL
UVW-smag3dpbl	3-D Smagorinsky applied only to velocity fields	YSU PBL
Initial conditions	2-D Smagorinsky and TKE initialized from organized state	YSU PBL

The initial horizontal homogeneous environment is specified based on Jordan mean hurricane sounding for the West Indies area [*Jordan*, 1958] which is subject to a humidity and pressure perturbation pattern in the initial state. To introduce heterogeneity an axisymmetric vortex anomaly in the temperature, humidity, and pressure is placed at the center of the domain which decreases radially and is applied for all vertical levels. The structure is a default initialization option in the WRF model and is described by *Rotunno and Emanuel* [1987]. To test the sensitivity to the initial conditions, a parallel set of 15 day integrations were conducted starting with small random perturbations to the temperature and humidity fields imposed on a uniform background state, using the smag3dpbl, tke3dpbl, and smag2dpbl schemes, respectively. These integrations confirmed the results of the main experiments and are not reported here. This is not to state that the initial conditions are not important, since additional experiments show that strongly organized states tend to remain organized (see section 3.3.3).

In addition to the above simulations, further ensembles of sensitivity simulations were conducted. In the first, the TKE scheme is employed and C_s increased systematically in each 15 day simulation to a maximum of 0.6, mimicking the 3-D Smagorinsky sensitivity simulations of *Takemi and Rotunno* [2003] which simulated a squall-line case. Further experiments attempt to isolate the impact of the humidity entrainment and investigate the sensitivity to strong organization in the initial conditions.

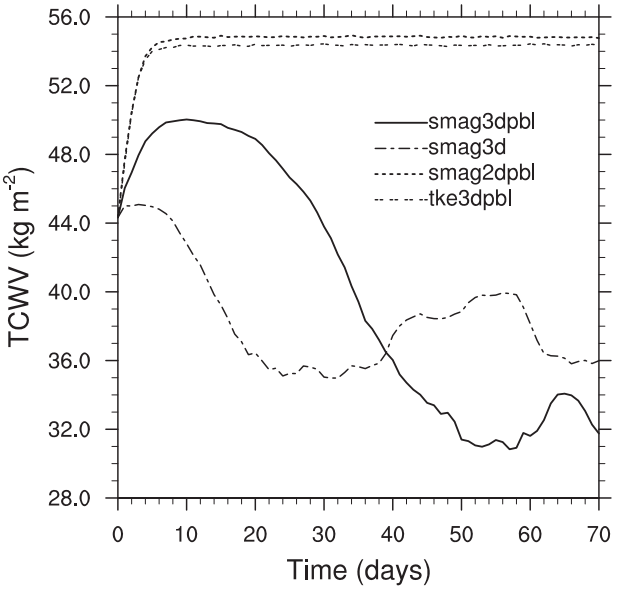


Figure 1. Time series of domain average total column integrated water vapor (TCWV, kg m^{-2}) for simulations smag3dpbl, smag3d, smag2dpbl, and tke3dpbl.

3. Results

3.1. Equilibrium States

The evolution of the domain mean, vertical integral of water vapor, referred to as the total column water vapor (TCWV) reveals the adjustment to equilibrium in the four simulations (Figure 1). In the two simulations using the 2-D Smagorinsky scheme and the TKE scheme (tke3dpbl and smag2dpbl), TCWV increases to a equilibrium value of 54 kg m^{-2} in around 5 days of integration and remains close to that level thereafter. No major temporal oscillations exceeding 1 kg m^{-2} are seen around the equilibrium state. In contrast, in the two simulations using the 3-D Smagorinsky scheme, the domain average TCWV significantly decreases to values in the range of 32–40 kg m^{-2}. The simulations reach equilibrium after around 30–40 days, the radiative-overturning adjustment time scale [*Tompkins and Craig*, 1998b; *Cronin and Emanuel*, 2013], but

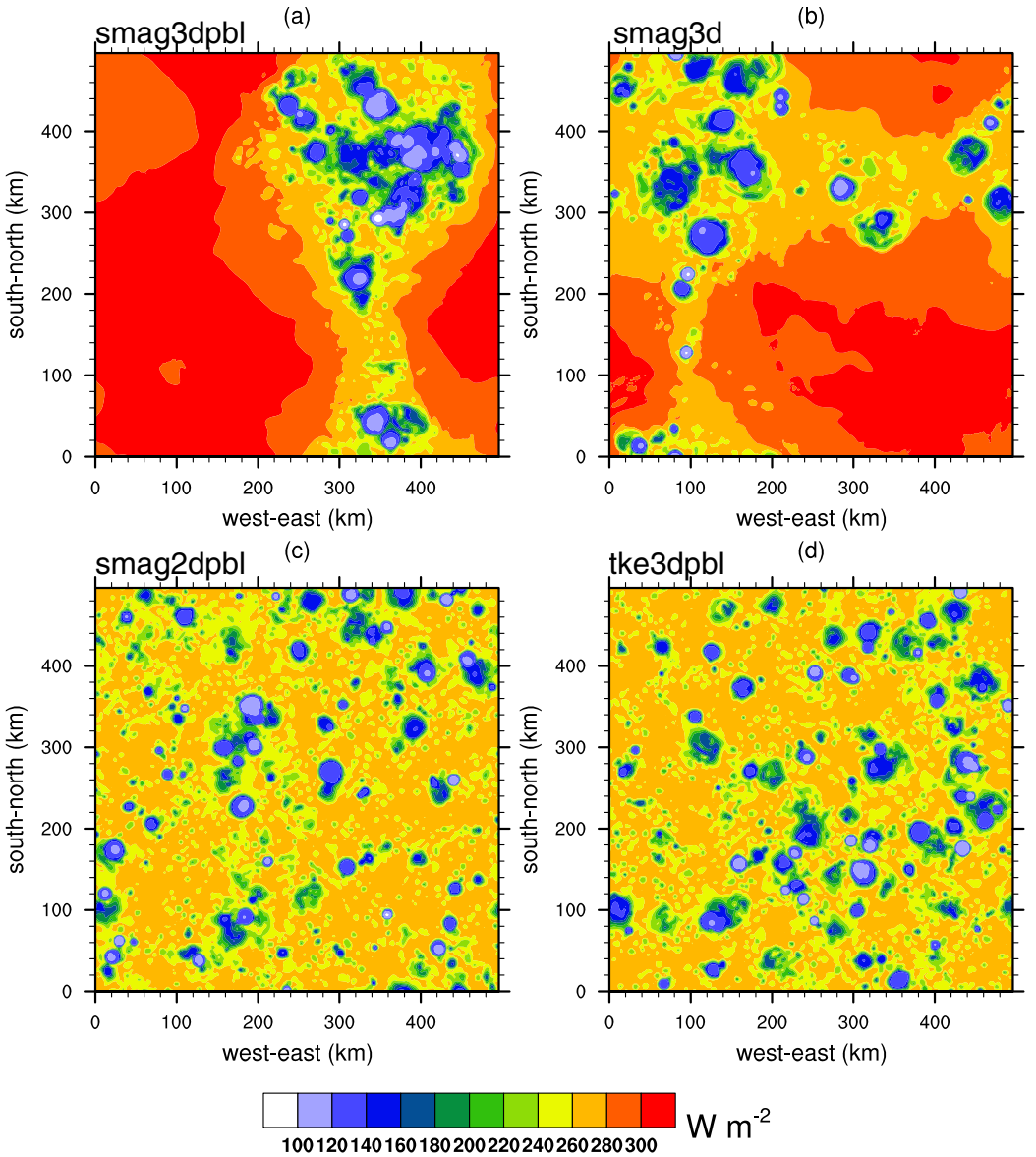


Figure 2. Top-of-atmosphere OLR on day 70 of the simulation for (a) smag3dpbl, (b) smag3d, (c) smag2dpbl, and (d) tke3dpbl.

oscillations occur around the equilibrium state. These characteristics of the smag3dpbl and smag3d simulations are an indication of the onset of self-organization, as organization leads to drier mean states [*Bretherton et al.*, 2005] and larger oscillations might be expected in highly organized states.

The state of organization at the end of each integration is derived from maps of top-of-atmosphere OLR (Figure 2). The two simulations using the 3-D Smagorinsky scheme evolve to an organized state, with cold convection anvils (OLR < 180 W m^{-2}) restricted to a single band within the domain, which changes orientation during the course of the simulations (not shown). In the band the OLR is between 260 and 280 W m^{-2}, and represents moist columns without high level cloud. The OLR is around 40 W m^{-2} higher in regions far from the convection, due to the extremely dry atmospheres that result from the organization. In contrast, tropospheric-deep convection continues to occur throughout the domain in the two simulations using the TKE and 2-D Smagorinsky scheme (tke3dpbl and smag2dpbl) and these high values of OLR are not observed.

The boundary between the moist and dry regions is very sharp in the simulations using the 3-D Smagorinsky scheme, resulting in two distinct modes in the TCWV probability density function (PDF) in the

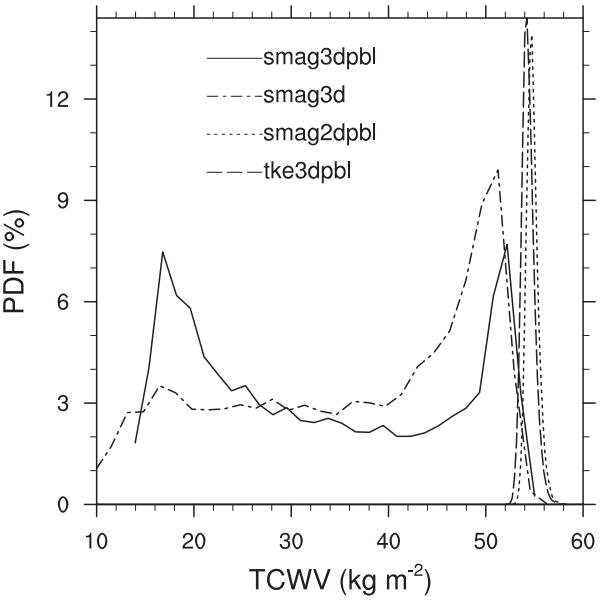


Figure 3. Probability density function of the total column water vapor (TCWV) for simulations smag3dpbl, smag3d, smag2dpbl, and tke3dpbl averaged over the final 5 days of the simulations.

simulations in which organization occurs (Figure 3). The moist regions are associated with a distinct moist mode; a distinct peak in the TCWV PDF for values exceeding 50 kg m^{-2}. The dry regions are marked by a second mode below 40 kg m^{-2}, which is much stronger in the simulation using the PBL scheme for vertical mixing. While previous work has noted bimodality in water vapor, this characteristic tends to be restricted to the upper troposphere detrainment zone [e.g., *Zhang et al*., 2003]. The strong gradients in humidity are likely exacerbated by the idealized simulation framework, where wind shear and rotation is absent by design. In the two simulations in which convection does not organize, the domain remains moister, as expected, and the PDF reveals a single moist mode.

Tephigrams show that the mean equilibrium structures are reasonable, although the representation of the well mixed boundary layer is poor in the smag3d scheme, which only represents local mixing (Figure 4). The large difference in the atmospheric moisture content between the organized and unorganized state is re-emphasized. Relative humidity is very high in both smag2dpbl and tke3dpbl below the freezing level. Interestingly, there is a distinct moist mode in the smag3dpbl integration in the 100 hPa layer below the freezing level; a possible indication of the trimodal detrainment level [*Johnson et al*., 1999; *Tompkins and Emanuel*, 2000; *Khairoutdinov et al*., 2009].

The level of organization is quantified by the time series of the organization index I_{org}, which reflects the evolution of the TCWV (Figure 5, see Appendix A for calculation). Simulations smag2dpbl and tke3dpbl, which evolved to a moist state, did not organize. Indeed, rather than being random, convection is slightly regular, as convective towers are slightly further apart on average than expected from a random distribution. The paired, nearest neighbor cumulative density function (NNCDF) curves for the duration of the simulations show that the regularity occurs over distances less than 19 km (Figure 6b), with the distribution of convective towers exactly random at scales exceeding this threshold. This is probably related to the effect of cold pools, which typically grow to radii of O(10km) in low shear environments [*Tompkins*, 2001c; *Ross et al*., 2004]. In such low wind shear conditions, cold pools trigger new convective updrafts at the gust front when they are mature and almost recovered, while preventing new convection from occurring in the direct vicinity of deep convection due to the suppression of the boundary layer virtual temperature, leading to mutual exclusivity [*Randall and Huffman*, 1980].

The two simulations using the 3-D Smagorinsky diffusion scheme show strong organization. Interestingly, the temporal evolution of the organization index I_{org} exactly mirrors that seen in the TCWV (Figures 1 and 5), which indicates that the multiday time scale oscillations of the domain mean water vapor around the equilibrium state are the direct result of oscillations in the degree of convective organization. Even in these simulations however, convection is regular at distances less than 15 km, while the clustering occurs over larger spatial scales exceeding this up to the domain size (Figure 6a).

The adjustment of the domain relative humidity (RH) as a function of height toward the organized state in simulation smag3dpbl mirrors the findings of *Tompkins and Craig* [1998b]. The wettest 10th percentile of the domain in terms of TCWV shows limited adjustment toward the equilibrium state, due to the moist initial conditions (Figure 7). In the driest 10th percentile, the adjustment is relatively fast in the deep convective detrainment zone between 12 and 14 km, where radiative cooling rates are decreasing with height toward the radiative tropopause at 14 km. Boundary layer fluxes and shallow convection keep the boundary layer moist for the first 2 weeks in this zone. Subsidence dries the troposphere in a "top-down" direction

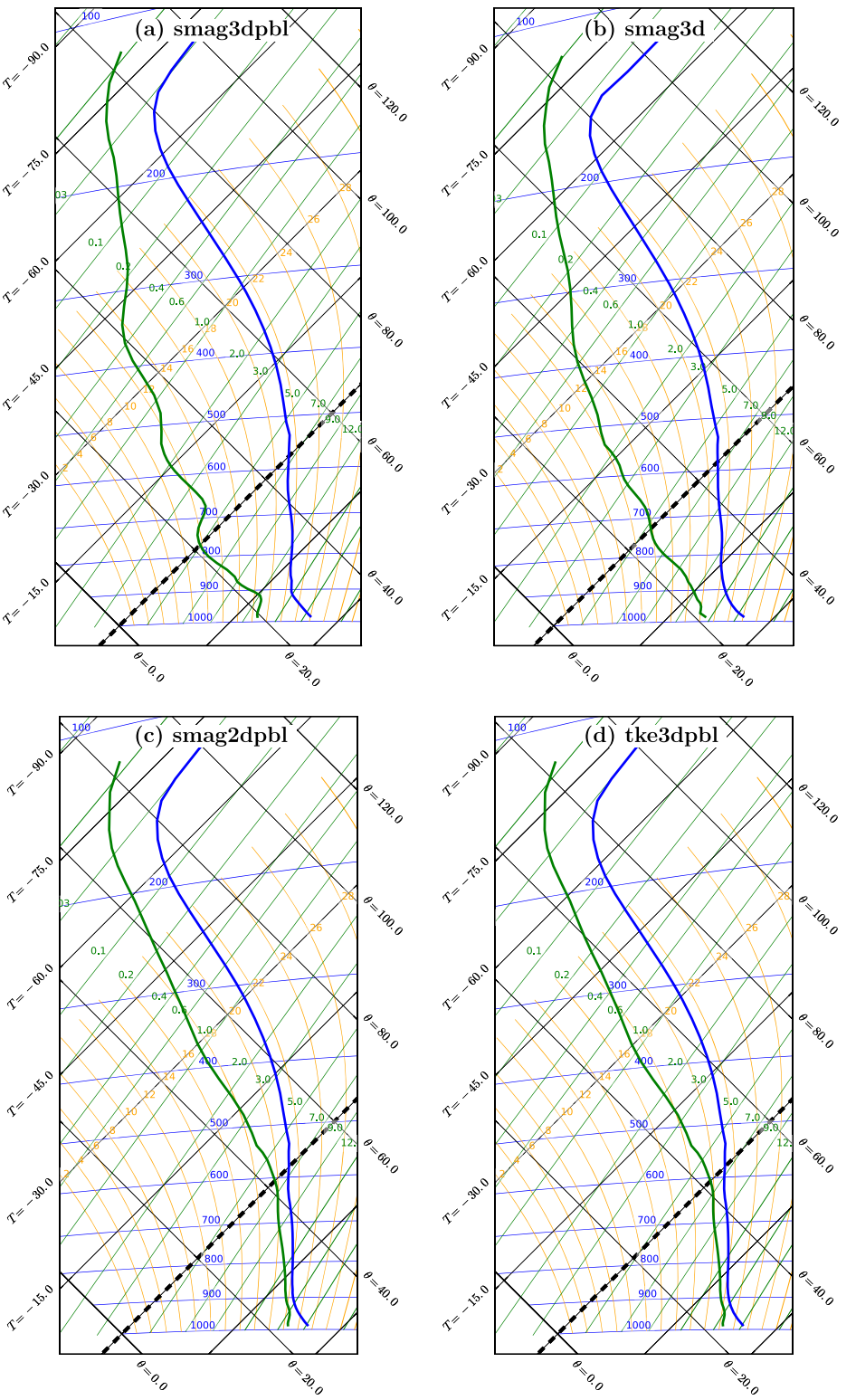


Figure 4. Tephigram charts of temperature (blue), specific humidity (green) for the final 5 day and domain mean average of the four experiments smag3d, smag3dpbl, smag2dpbl, and tke3dpbl. In tephigrams, the near horizontal lines are pressure (blue), the black diagonal lines are isopleths of T and θ, the green diagonal lines are isopleths of saturation mixing ratio and the curved lines are isopleths of θ_e.

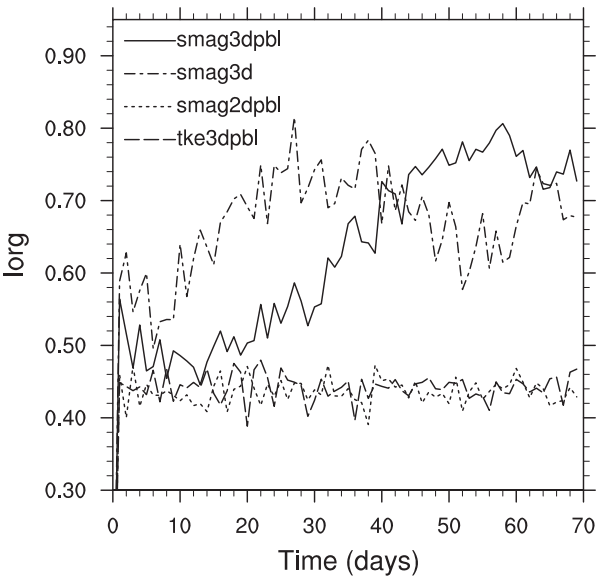


Figure 5. Organization index (I_{org}) sampled once daily for simulations smag3dpbl, smag3d, smag2dpbl, and tke3dpbl (see legend).

shortly after the onset of organization, as expected since the lateral convective source of water vapor (via detrainment) becomes more remote as organization progresses [see *Pierrehumbert and Yang*, 1993; *Yang and Pierrehumbert*, 1994; *Couhert et al*., 2010; *Sherwood et al*., 2010].

The adjustment to an organized state can also be examined in terms of the domain standard deviation of the relative humidity (with smag3dpbl and smag2dpbl shown in Figure 8). As the initial conditions for the simulations contain a strong perturbation in temperature and humidity in the initial vortex structure, the convection occurs predominantly in the central part of the domain immediately after initialization. This increases the RH variance in the mid-to-upper troposphere in both simulations during the first 2–3 days, which then decreases as deep convection propagates throughout the domain. The simulations start to diverge after day 3, however, with RH variance increasing throughout the lower troposphere in the simulation using the 3-D Smagorinsky mixing scheme. The variance increases fastest after day 20 as the deep convection organizes, reaching equilibrium after 35 days. In this state, the maximum variance of RH occurs at two levels, at 1–2 km height above the planetary boundary layer and at 4 km height below the freezing level mode. In contrast the RH variance remains limited at all levels in smag2dpbl after day 10.

The net radiative heating rates in simulation smag3dpbl are divided into four quartiles to show the contrasts between the driest and wettest parts of the domain (Figure 9). As discussed in *Wing and Emanuel* [2013] and *Emanuel et al*. [2014], as organization develops, the driest quartile is subject to the greatest net cooling rates throughout the mid-to-upper troposphere, encouraging greater subsidence and convergence into the moister regions. As the organization increases, the driest quartile becomes so dry that its net cooling rate decreases in the mid-to-upper troposphere, and it is actually the intermediate quartiles that have the greatest cooling rates. The driest quartile instead has the greatest cooling rates in the boundary layer due to the dryness of the atmosphere above, which are offset by increased turbulent fluxes in that layer. The observed structures in the radiative cooling rates confirm the assumptions of the two-layer model in *Emanuel et al*. [2014], which were based on simulations using a different cloud-resolving model.

3.2. Role of Mixing

The results of the four simulations clearly show that horizontal mixing is a key factor for determining the occurrence of convective organization. The only difference between the sensitivity simulations of smag3dpbl, smag2dpbl, and tke3dpbl is the representation of horizontal subgrid mixing since all three simulations employ the same approach for vertical mixing.

The mixing strength is quantified by the horizontal eddy viscosity or mixing coefficient k_h as described by equations (1)–(3) for the cases of 2-D Smagorinsky, 3-D Smagorinsky and TKE closure schemes, respectively. At a height of 500 hPa using the 3-D Smagorinsky and TKE schemes, the eddy mixing is mostly taking place in the vicinity of convective cores, due to the horizontal gradients in vertical velocity there (Figure 10). In most of the domain away from convective cores, the mixing coefficient adopts the imposed minimum value of 4 $m^2\ s^{-1}$. Instead values on the order of 50–100 $m^2\ s^{-1}$ are found throughout the domain for the 2-D Smagorinsky scheme. Away from cores, the $\frac{dw}{dx}$ and $\frac{dw}{dy}$ terms are small, thus only difference between the 2-D and 3-D Smagorinsky schemes away from cores is that the latter accounts for static stability, which suppresses turbulence in the free troposphere. The static stability is accounted for in the TKE prognostic equation also suppresses free tropospheric mixing in that scheme.

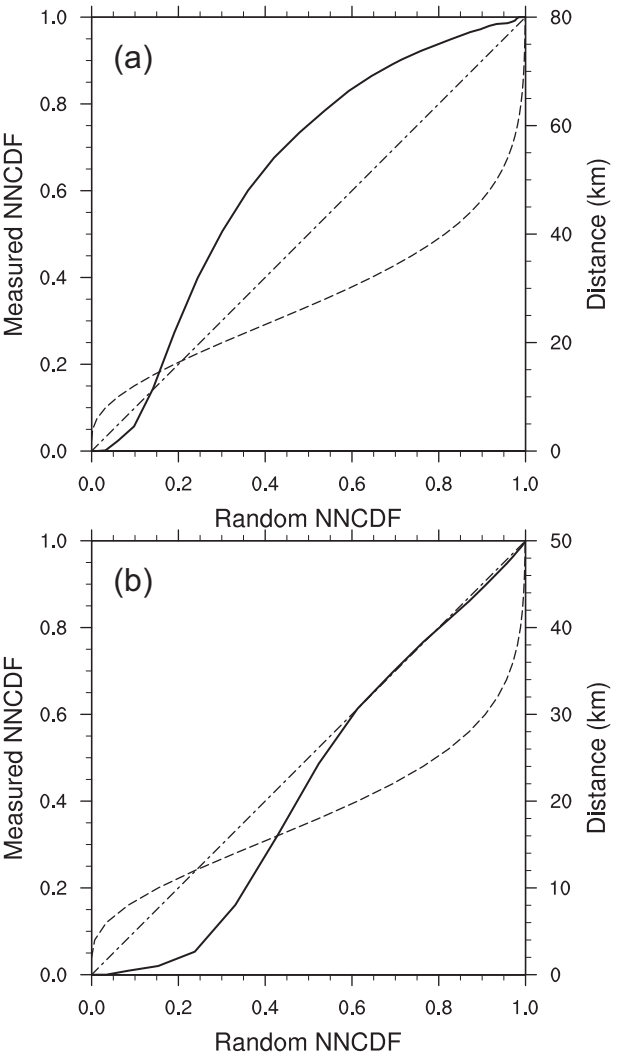


Figure 6. Solid line: Model NNCDF (left *y* axis) against Poisson NNCDF (see Appendix A for calculation method) for (a) smag3dpbl and (b) smag2dpbl. The dashed line indicates spatial scale (right *y* axis, read vertically down from the solid to the dashed line to obtain the spatial scale for each NNCDF point). Simulations smag3d and tke3dpbl (not shown) are almost identical to smag3dpbl and smag2dpbl, respectively.

The slice of k_h at 500 hPa shows the diagnostic nature of the 3-D Smagorinsky scheme leads to very high mixing only at the updraft core itself, where the horizontal shear of the vertical velocity is large (Figures 10a and 10b). The prognostic TKE scheme produces much lower peak mixing values, but the transport of TKE leads to higher mixture over a large radius of grid cells surrounding the updrafts (Figure 10d).

A comparison of the eddy viscosity k_h calculated for the domain mean and all updraft cores with vertical velocity exceeding 1 m s^{-1} indicates stark differences in the magnitude of the mixing between the approaches (Figure 11). The neglect of the static stability leads to the domain mean mixing coefficient being approximately constant with height when using the 2-D Smagorinsky scheme (Figure 11a). Instead mixing decreases strongly with height in both the 3-D Smagorinsky and TKE schemes due to the impact of static stability and the reduction in the number of convective cores. The simulations with the 3-D Smagorinsky scheme, smag3dpbl, and smag3d, have an order of magnitude greater horizontal mixing coefficient compared to the smag2dpbl and tke3dpbl simulations in the lower troposphere below 800 hPa (Figure 11). Above 800 hPa, the domain mean mixing is lower than that of the TKE scheme, while the average of the convective grid cell only is higher, again emphasizing the impact of the prognostic approach relative to the diagnostic, local Smagorinsky scheme. TKE is advected in WRF, and mixing strength is consequently higher in the upper troposphere. It is also noted that the domain mean, mass-weighted vertical integrals of the TKE and 3-D Smagorinsky mixing coefficients are not equal, highlighting the fact that despite the two schemes accounting for shear and stability similarly, the Smagorinsky approach is not simply a local diagnostic equilibrium version of the TKE scheme.

Comparing the TKE and 3-D Smagorinsky approaches, while the schemes both account for the same processes of stability and shear, the 3-D Smagorinsky scheme diagnoses far higher mixing rates in the locality of the updraft cores. It is recalled that the use of 3-D Smagorinsky leads to organization, while the TKE does not. The greater mixing in the 3-D Smagorinsky scheme suggests that updraft entrainment processes in the lower troposphere are key, and that sufficiently large entrainment is required for organization to occur. If entrainment is relatively low, convection can occur in the drier regions of the domain, thus acting as a negative organizational feedback and destroying nascent organization by locally moistening the dry perturbations through detrainment processes. The significant differences in the domain mean mixing between the 3-D Smagorinsky and TKE approaches highlight the importance of the dissipation term in the TKE equation, which is a function of the atmospheric stability (see section 4.2.4 of *Skamarock et al.* [2008]).

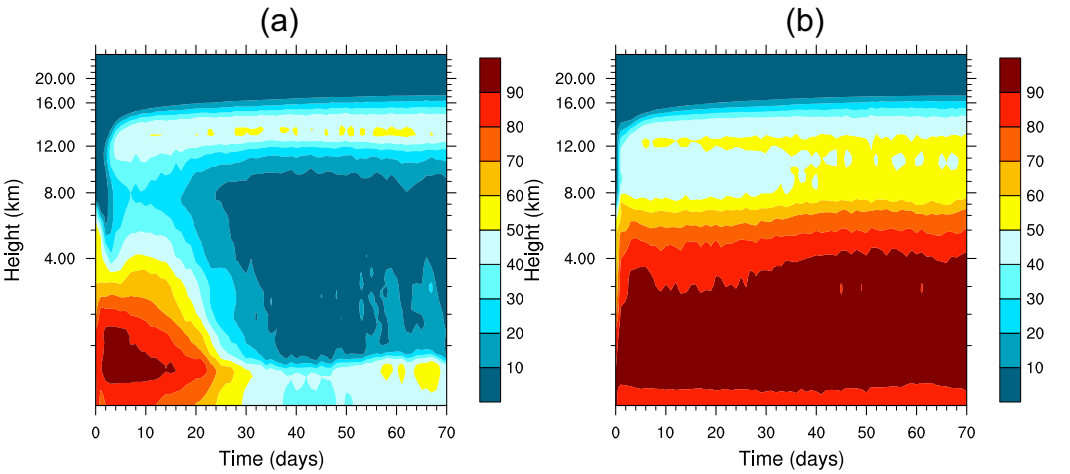


Figure 7. Relative humidity as a function of height for the (a) driest and (b) moistest 10th percentile of TCWV, showing the adjustment to equilibrium in smag3dpbl.

3.3. Sensitivity Experiments

3.3.1. Humidity Entrainment Experiment

The use of the 3-D Smagorinsky scheme leads to the onset of organization, and it is suggested that this is due to the stronger mixing in the vicinity of updraft cores that this scheme diagnoses. The entrainment of dry air would reduce updraft buoyancy and suppress updraft momentum [*Derbyshire et al.*, 2004], thus it is suggested that the organization results specifically from the strong entrainment of humidity, rather than momentum. To test this hypothesis, two further simulations were conducted for a period of 45 days. In the first simulation (TQ-smag3dpbl), only the scalar quantities of temperature and humidity are horizontally mixed by the Smagorinsky scheme, while the mixing of all other parameters is zero. In the second simulation (UVW-smag3dpbl), the velocities field is horizontally mixed, while scalar mixing is neglected. As expected, the TQ-smag3dpbl simulation tracks the full smag3dpbl simulation, while the simulation with velocity mixing (UVW-smag3dpbl) remains unorganized (Figure 12). This sensitivity experiment confirms the hypothesis that it is the horizontal entrainment of humidity into the convective updrafts that is key.

3.3.2. Eddy Strength Experiment

It is postulated that the TKE simulation did not produce convective organization since the entrainment mixing was too weak to prevent convection from removing dry perturbations, even though the horizontal shear of the vertical wind velocity is accounted for in the prognostic TKE equation. A testable prediction resulting from this hypothesis is that amplifying the eddy mixing in the TKE scheme should result in the

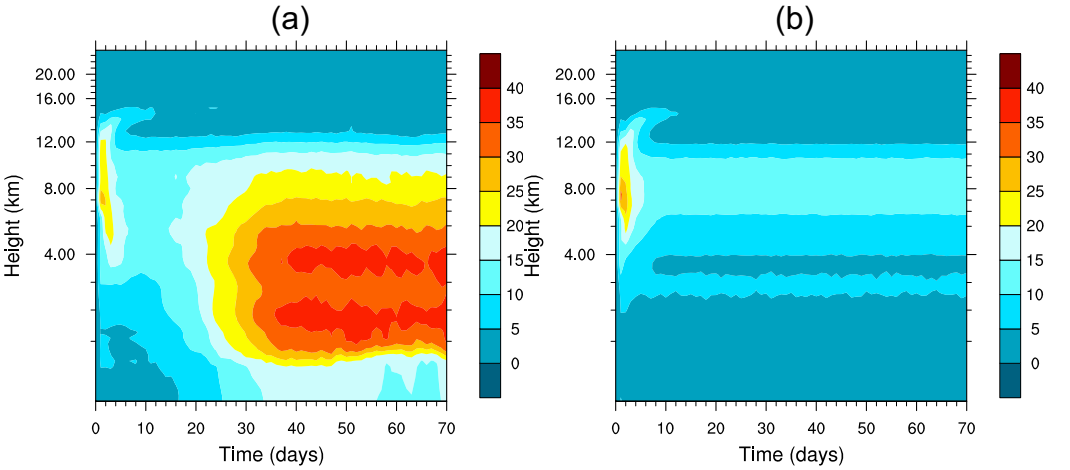


Figure 8. Temporal evolution of the spatial standard deviation of relative humidity in the (a) smag3dpbl and (b) smag2dpbl simulations.

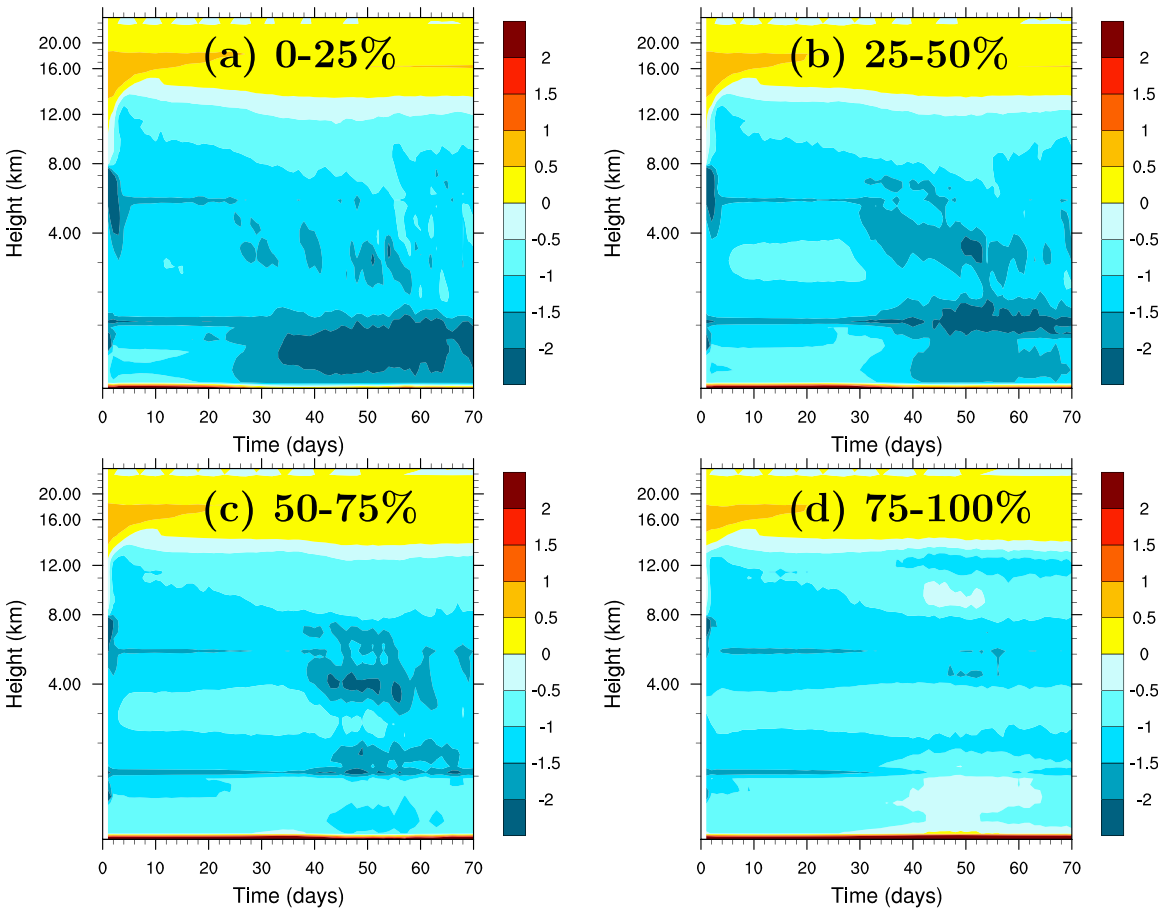


Figure 9. Net radiative heating rates for simulation smag3dpbl averaged over the (a) driest quartile (b) second quartile (c) third quartile, and (d) moistest quartile according to the column integrated water vapor.

onset of organization. This amplification is achieved by increasing the eddy mixing coefficient C_s, which is a crude measure of the mixing efficiency of the largest subgrid-scale eddies, and is typically between 0.15 and 0.23. In the control simulations the value of 0.15 was used, but a set of five additional sensitivity 15 day simulations was conducted in which the value was set to 0.2, 0.3, 0.4, 0.5, and 0.6. Thus, the most extreme simulation increases the eddy mixing by a factor of 4, closer to the mixing strength diagnosed by 3-D Smagorinsky approach in the vicinity of convective updrafts.

The organization index for these simulations appears to confirm the hypothesis (Figure 13). Simulations with small enhancements in mixing do not undergo organization, but at a mixing coefficient of 0.5 the system switches to an organized state within 15 days. This transition is very apparent in Figure 14, which shows the enhanced mixing value in the latter two simulations in the neighborhood of cores which occupy an increasingly smaller fraction of the domain as the mixing coefficient is increased.

3.3.3. Initial Conditions Sensitivity

To test the sensitivity of the convective organizational state to initial conditions, two further simulations were conducted. In the first, the smag3dpbl, tke3dpbl, and smag2dpbl simulations were started from a resting initial state with small random perturbations applied to the temperature, humidity, and velocity. The magnitude of the perturbations is similar to those applied in the vortex initialization, thus the key difference is in the spatial structure of the perturbation pattern. The 3-D Smagorinsky scheme still resulted in an organized state, in contrast to the other two experiments, indicating that the spatial pattern of the perturbations had a limited effect (not shown).

A second experiment instead used the organized state on day 70 of the smag3dpbl integration as initial conditions for three further simulations, using the PBL scheme for vertical mixing and the TKE scheme, the 2-D Smagorinsky scheme, or the 3-D Smagorinsky applied only to momentum fields for horizontal mixing

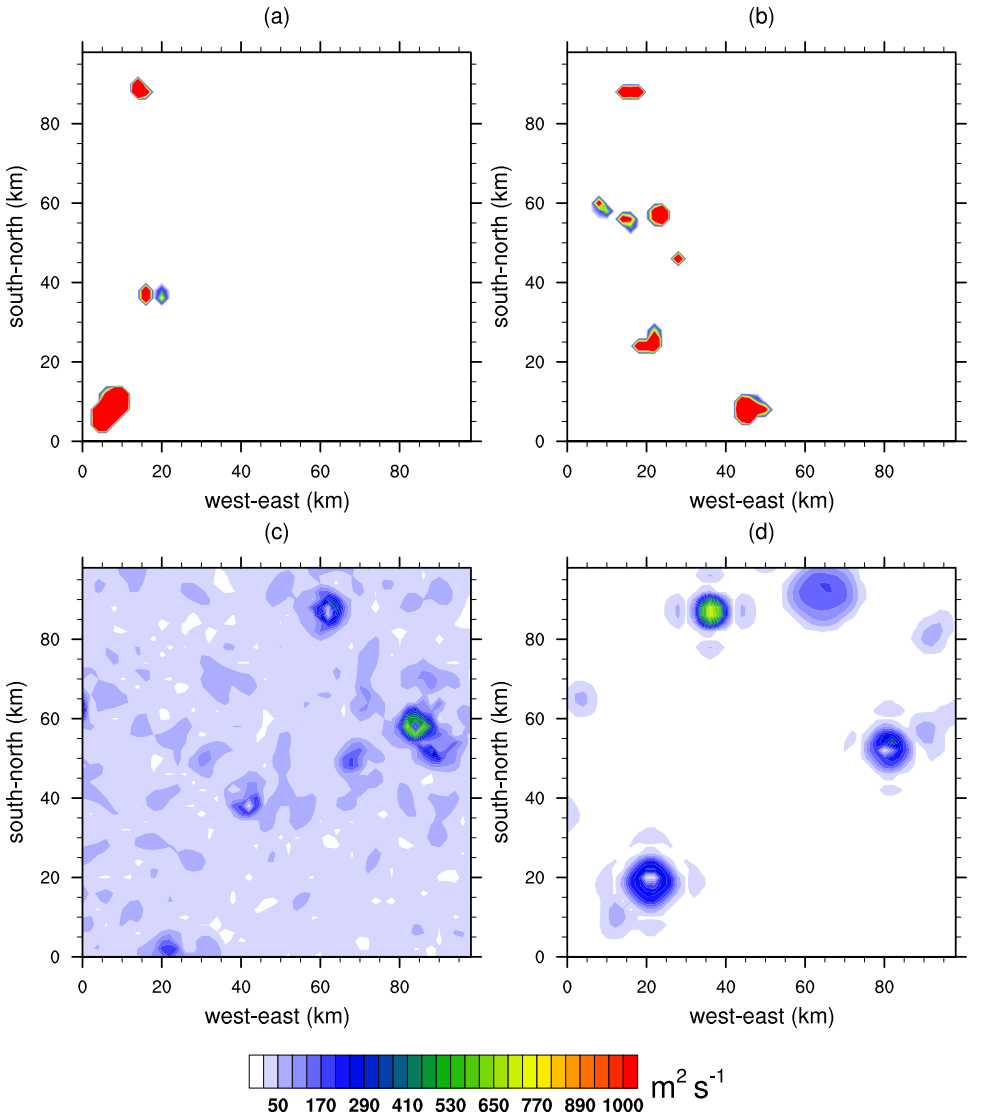


Figure 10. k_h at 500 hPa within an arbitrarily chosen subdomain of 100 km by 100 km containing deep convection on the final day of simulation for (a) smag3dpbl, (b) smag3d, (c) smag2dpbl, and (d) tke3dpbl.

(tke3dpbl, smag2dpbl, and UVW-smag3dpbl, respectively). These three experiment configurations were chosen since they all prevented convective organization from occurring, and thus they may be expected to lead to the breakup of the organized state within the 30 day integration period (the radiative overturning time for the free troposphere, *Tompkins and Craig* [1998b]). In fact, Figure 15 shows that despite strong oscillations in the degree of the organization, the simulations remain organized, revealing a strong hysteresis behavior.

It is clear why this hysteresis may occur, since the suppression of buoyancy in updrafts is related not only to the strength of the entrainment mixing, but also to the magnitude of the humidity anomaly of the air entrained. Thus, even the weaker entrainment mixing of the default TKE and 2-D Smagorinsky turbulence schemes is adequate to suppress deep convective activity if occurring in very dry regions, as is the case when initializing the model with an already organized state. Moreover, in the organized state, the boundary layer is also drier, reducing convective available potential energy and increasing convective inhibition energy. It is noted that this result contrasts with the findings of *Tompkins and Craig* [1998a], who found that homogenizing radiative heating rates or surface fluxes quickly destroyed organization within 4 days of integration. However, *Tompkins and Craig* [1998a] used a small domain size of O(100km) which limits the

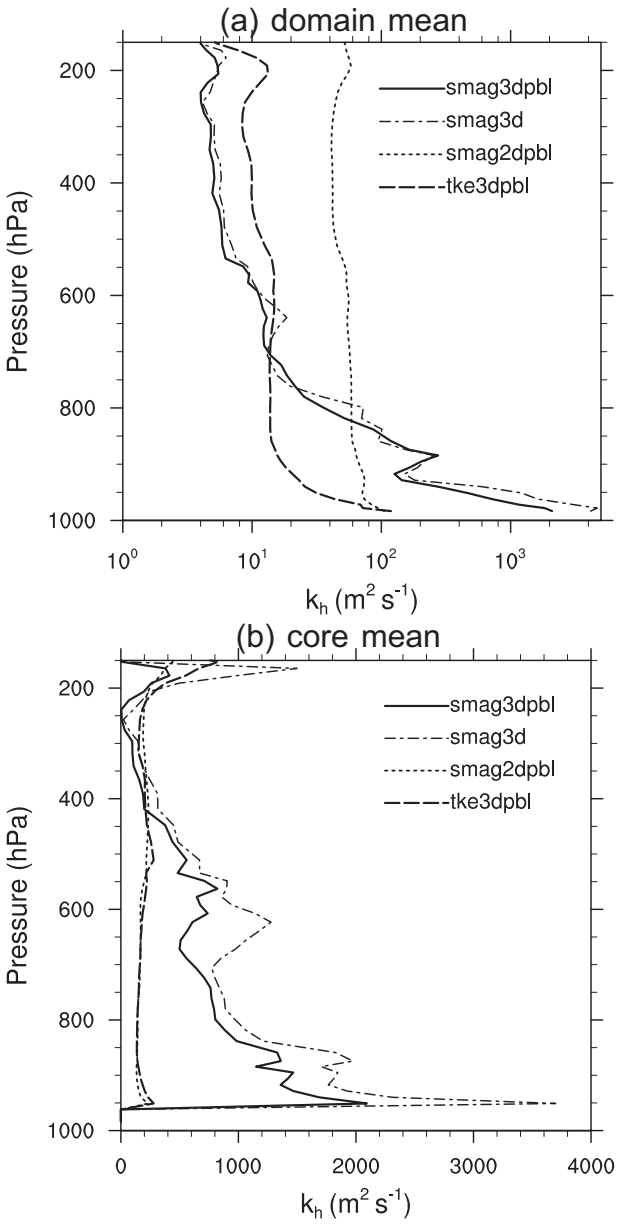


Figure 11. Vertical profile of the mean the horizontal mixing coefficient k_h calculated for the (a) domain mean and (b) all updraft cores, defined as grid cells with vertical velocity exceeding 1 m s^{-1}. The simulations are given the legend.

distance between convective clusters, and thus also the variability of humidity possible within the domain. Indeed, *Muller and Held* [2012] found O(100km) domain sizes prevented convective organization from occurring altogether.

4. Discussion

Emanuel et al. [2014] introduced a simple two-layer model to investigate how radiative feedback with water vapor may lead to instability. The model successfully represents the respective roles of the upper and lower tropospheric emissivity in convective organizational feedback, which was demonstrated in *Wing and Emanuel* [2013]. Concerning the water vapor convection feedback in a variant of their simple model, *Emanuel et al*. [2014] noted that "the sensitivity of convection to water vapor boosts the instability but cannot destabilize the model on its own." It is important to emphasize that this conclusion is an outcome of the physical assumptions on which the simple model is based and may not reflect the behavior of the tropical atmosphere. The two-layer model of *Emanuel et al*. [2014] determines the convective mass flux using the boundary layer quasi-equilibrium theory of *Raymond* [1995] and *Emanuel* [1995]. Water vapor affects the convective mass flux, but only because with a drier midtroposphere, less mass flux is required to provide the necessary moist static energy flux from the boundary layer (see their equation (14)). In other words, no matter how dry the troposphere is, entrainment cannot inhibit convection in that model, and it is consequently logical that water vapor-convection feedback plays a limited role in its instability. This is not supported by numerical experimentation [*Tompkins*, 2001a; *Derbyshire et al*., 2004; *Grabowski and Moncrieff*, 2004], with the strong caveat that these simulations used large grid sizes O(2km), which is discussed further below.

The potential role of entrainment can be illustrated it by considering a two column representation of the tropics in a state of radiative-convective equilibrium (RCE). The weak temperature gradient (WTG) approximation is assumed to hold, in which gravity waves remove virtual temperature perturbations efficiently [*Sobel et al*., 2001; *Polvani and Sobel*, 2002] and convective activity is equal in both columns, with the compensating subsidence balancing radiative cooling (see schematic in Figure 16). The response to a dry perturbation in one column is considered, assumed to be in the mid-to-upper troposphere (refer to Figures 7 and 8). As discussed in *Emanuel et al*. [2014] and *Wing and Emanuel* [2013], the response to the drying would be enhanced long-wave radiative cooling in the troposphere below the dry perturbation, with reduced cooling aloft (as seen in Figure 9).

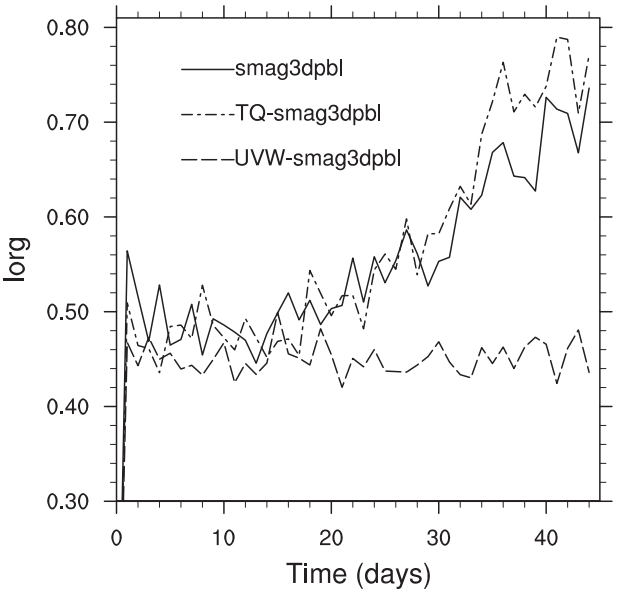


Figure 12. Organization index I_{org} for the first 45 days of the smag3dpbl simulation, compared to two sensitivity tests in which the 3-D Smagorinsky mixing scheme is applied only to scalars (TQ-smag3dpbl) or velocity fields (UVW-smag3dpbl).

How would the two column system respond to these perturbations? The WTG assumption dictates that the enhanced cooling must be offset by enhanced subsidence to prevent horizontal buoyancy gradients, but the corresponding enhancement of deep convection can occur in either or both columns. If deep convection is highly sensitive to the dry environment through an entrainment mechanism, whereby the evaporative cooling effectively nullifies updraft buoyancy, then the enhanced convective mass flux will occur in the moister column. While deep convection dries the atmosphere (precipitation is produced), locally it moistens the environment through detrainment, while the drying is spread over the deformation radius through gravity wave propagation [*Bretherton and Smolarkiewicz*, 1989]. Thus, in this situation, the horizontal gradient of the total column water vapor is increased by enhanced convective detrainment in the moist column (see discussion in *Grabowski and Moncrieff* [2004], which also highlights the potential additional role that precipitation evaporation can play to further strengthen this feedback). This represents a positive organizational feedback that could lead to a situation where all deep convective activity occurs in one column only. This is the situation in the simulations reported here when the 3-D Smagorinsky mixing scheme is used, leading to a high sensitivity of convection to environmental moisture.

If the entrainment into convective updrafts is limited, then the dry perturbation will have minimal impact on deep convection through entrainment. Any imbalance in convective mass fluxes between the two columns will only be due to the response to the radiative cooling in each column, where the dry patch will enhance radiative cooling in the layer below [see *Sherwood et al*., 2010; *Wing and Emanuel*, 2013; *Emanuel et al*., 2014]. Any nascent dry perturbation is eradicated by local detrainment and convection remains unorganized. This was the situation with the 2-D Smagorinsky and TKE turbulence schemes in our simulations, which produced smaller mixing rates near updraft cores in the mid-to-lower troposphere. It is likely that the entrainment sensitivity has to be high for spontaneous organization to occur, since the dry patches grow downward from the upper troposphere, where there is relatively little water vapor. *Sherwood et al*. [2010] highlights how the evidence for lower to midtropospheric water vapor control on convection is substantial, while the existence of the influence of upper tropospheric water vapor anomalies, such as suggested by *Waugh and Polvani* [2000], is unclear.

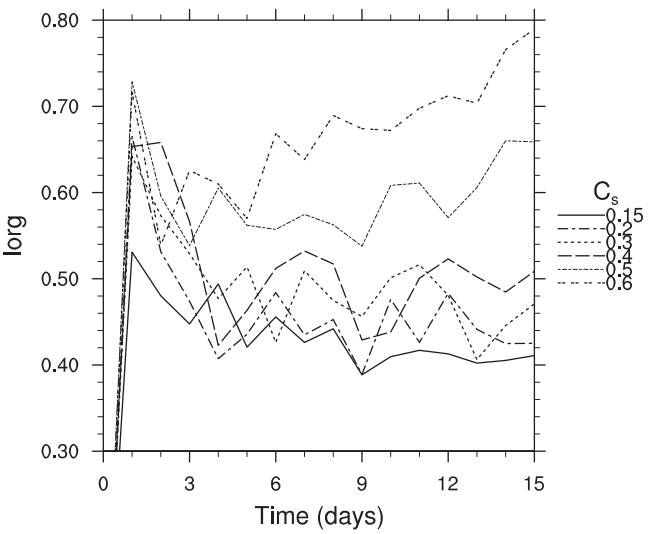


Figure 13. Daily sampled organization index (I_{org}) using the TKE turbulence scheme with C_s values of 0.15 (default simulation tke3dpbl), 0.2, 0.3, 0.4, 0.5, and 0.6.

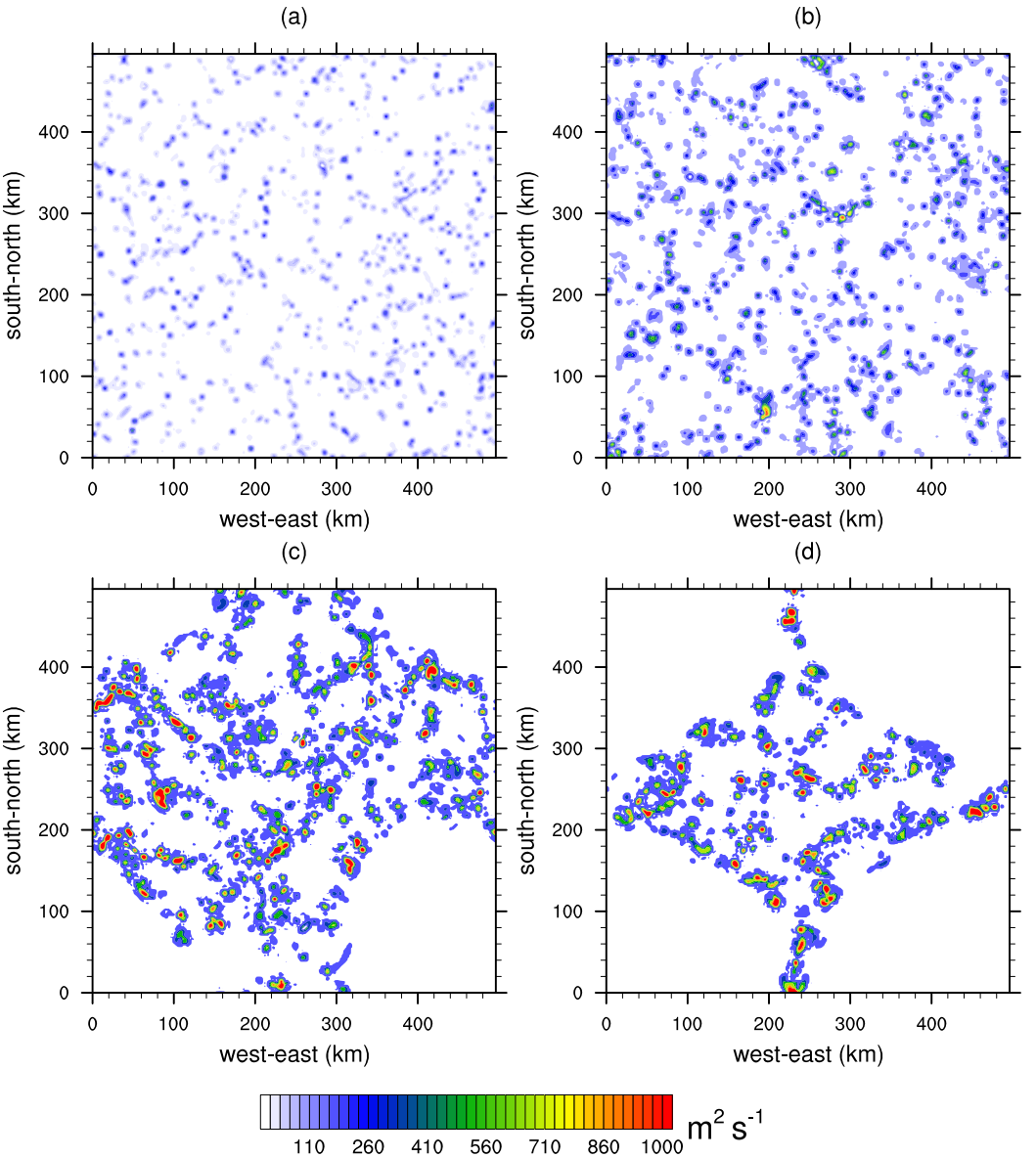


Figure 14. Horizontal slice of k_h at 950 hPa for C_s values of (a) 0.2, (b) 0.3, (c) 0.4, and (d) 0.5 at day 15 of the TKE sensitivity experiment simulations.

What do these results imply about the findings of previous studies? As stated in the literature review *Pauluis and Garner* [2006] and *Muller and Held* [2012] both investigated the sensitivity of spontaneous organization to the horizontal resolution employed in the models. *Muller and Held* [2012] stated that a grid size coarser than 2 km was required for convective organization to occur. The results here suggest that this could be partly attributable to the strength of entrainment mixing represented by the subgrid-scale scheme. Subgrid-scale parameterization schemes for turbulent mixing usually contain a parameter that represents the eddy length scale, which (above the PBL) is often related to the model grid size. At finer resolutions the eddy mixing length will be smaller. If numerical and explicit mixing of air into the updraft does not increase to compensate, then entrainment, and consequently convection feedback with water vapor, will decrease at finer resolutions. Finer resolution models could therefore be less likely to undergo spontaneous organization, as seen in *Muller and Held* [2012]. Organization in global model simulations of RCE will thus also be sensitive to the convective

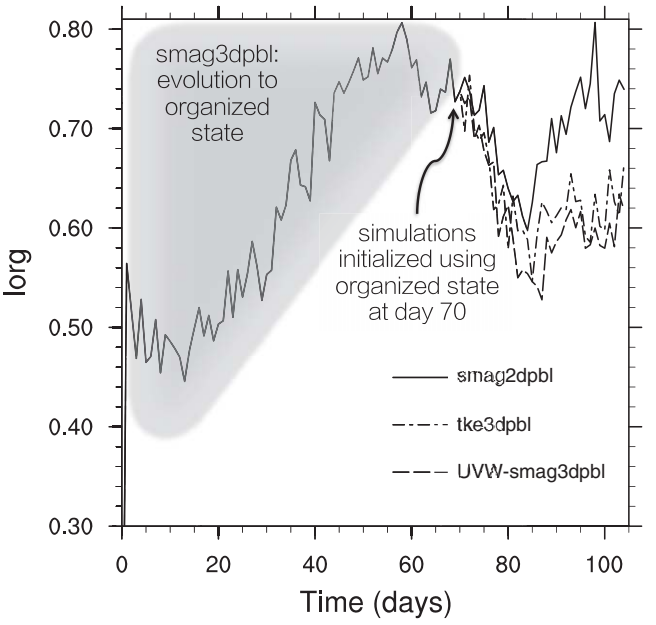


Figure 15. Time series of organization index I_{org}, showing smag3dpbl for the first 70 days. At day 70, the organized convective state is used to initialize three simulations, smag2dpbl, UVW-smag3dpbl, and tke3dpbl, which are integrated for a further 30 days.

parameterization scheme's entrainment formulation [e.g., *Popke et al.*, 2013; *Reed et al.*, 2015; *Coppin and Bony*, 2015].

The neglect of the horizontal shear of the vertical velocity in the 2-D Smagorinsky scheme would imply that the TKE or 3-D Smagorinsky schemes represent mixing with more fidelity, but evaluating the respective schemes is not straightforward as even the definition of entrainment is still debated [*Romps*, 2010; *Sherwood et al.*, 2013; *Yeo and Romps*, 2013; *Dawe and Austin*, 2013; *De Rooy et al.*, 2013]. Indeed, *Bryan et al.* [2003] pointed out that subgrid closures designed for large-eddy simulations are not valid at O(1km) spatial scales, suggesting that 100 m or finer grid sizes are required. Even with an accurate magnitude of mixing, at 2 km grid sizes, any entrained air is mixed uniformly throughout the updraft in a similar manner to the bulk mass-flux parameterization schemes that use a top-hat approach [e.g., *Tiedtke*, 1989], a deficiency that is in conflict with observations of stochastic, episodic mixing in clouds [*Paluch*, 1979] that motivated efforts to improve convective parameterization approaches *Emanuel* [1991], *Emanuel and Zivkovic-Rothman* [1999], and *Romps* [2016]. The use of such coarse resolutions in cloud-resolving studies of RCE prevents undilute updrafts to penetrate to the upper troposphere. While *Romps and Kuang* [2010] question the amount of undilute mass flux that reaches the convective detrainment zone, their study still diagnoses a significant undilute mass-flux proportion in the lower to midtroposphere. We surmise that homogeneous mixing of air through the updraft core may artificially suppress convection and enhance organizational feedback as a result.

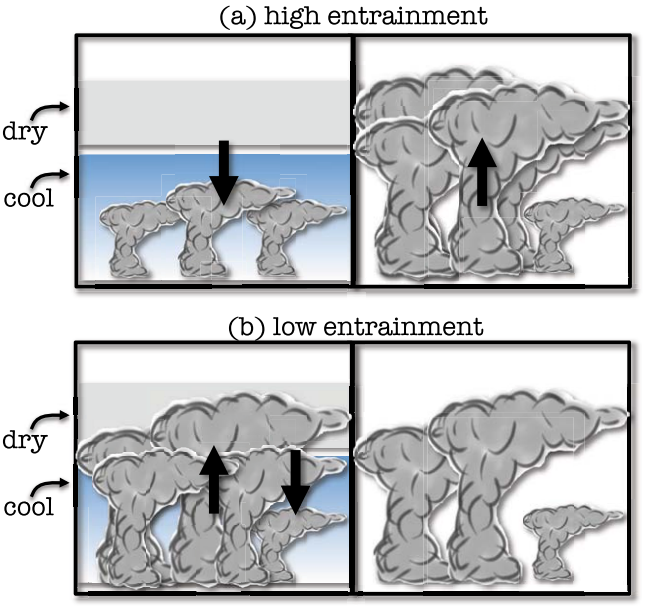


Figure 16. Schematic of the possible responses to a upper troposphere dry perturbation in a two column model of RCE. (a) With high convective sensitivity to entrainment of dry air the convection will be enhanced in the moist column (black arrows), and a positive organizational feedback occurs. (b) In contrast, low entrainment sensitivity leads to convection removing the dry perturbation locally and convection does not organize. See main text for full discussion.

Is there evidence that 2 km cloud-resolving models of RCE could be exaggerating the strength and extent of organization? It is certainly the case that in models that undergo organization, the dry regions in which convection is suppressed are extremely dry when compared to observations in the tropics. Part of the reason could be the lack of domain-scale eddies driving mixing at the mesoscale in the idealized frameworks that often employ period lateral boundary conditions as here, it could certainly be the case that

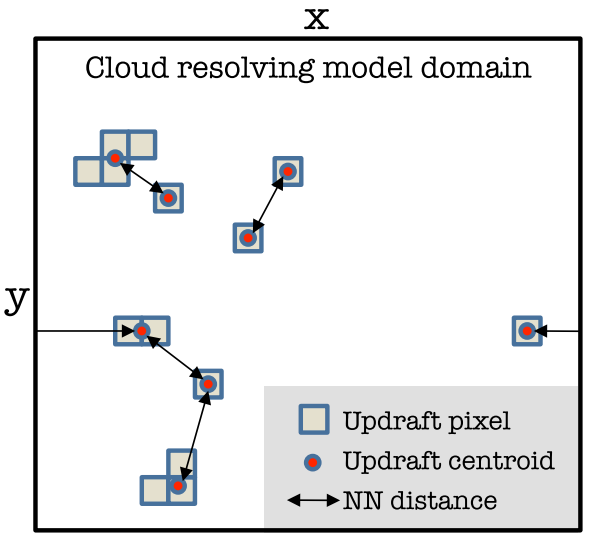


Figure 17. Schematic of NNCDF calculation. The domain is recursively traced to identify the geometric centroid of each updraft (red points) and the distance to its nearest neighbor is calculated (double headed arrows). The NNCDF is the normalized cumulative density function of these distances.

an exaggeration of the positive organizational feedback strength could be enhancing the moist-dry gradients.

5. Conclusions

Numerical models of the atmosphere that use convection-permitting horizontal resolutions have proven themselves to be very useful tools for understanding the potential for convection to organize spontaneously. Studies with such models have often, but not always, shown spontaneous organization of convection to occur. While many spatial feedback mechanisms have been investigated to ascertain their role in organization, no definitive picture has yet been obtained. Part of the reason for this is likely to be that the relative roles of radiative, water vapor, cloud and convection thermodynamical and dynamical interactions will be a strong function of the model's physical parameterizations for microphysics and turbulence, in addition to the experimental framework chosen, such as domain size and strength of imposed background wind (shear).

Here a cloud-resolving model was integrated to radiative-convective equilibrium using a domain of 500 by 500 km with a horizontal resolution of 2 km in four separate simulations, each of which used a different set of parameterizations to represent horizontal and vertical subgrid-scale mixing. In two of the simulations, convection strongly organized, whereas in two others it remained close to being random (in fact, the convection was slightly regularly spaced, due to the mutual exclusivity of cold pools at spatial scales inferior to 15–20 km). The key difference between these simulations was the strength of the horizontal subgrid-scale mixing in the vicinity of updraft cores. Using a diagnostic 3-D Smagorinsky scheme, the mixing was much stronger than the standard 2-D Smagorinsky scheme, due to the $\frac{dw}{dx}$ and $\frac{dw}{dy}$ horizontal shear of the vertical wind component terms. The prognostic turbulence kinetic energy (TKE) scheme account for this shear term, but the transport and dissipation terms result in less mixing in the lower troposphere, and specifically, between updrafts and their environment, and no organization resulted.

Greater subgrid-scale mixing drives greater subgrid-scale entrainment into the updraft cores (homogeneously throughout the core at O(2km) grid sizes) implying a stronger water vapor-convection feedback, and allowing spontaneous organization to occur. We use the term "allowing," since radiative-convective feedbacks are still key in driving the strong organization, as shown previously by *Tompkins and Craig* [1998a], *Stephens et al*. [2008], *Wing and Emanuel* [2013], and *Emanuel et al*. [2014]. The simulations here show that water vapor feedback with convection does not just have the potential to amplify organization driven by other mechanisms; it is a *necessary but not sufficient condition* for convective organization. While the diabatic budget analysis methodology of *Wing and Emanuel* [2013] is useful for diagnosing the relative contributions of processes to the formation and maintenance of the organized state, it is always important to recall that these budgets are a function of the physical assumptions contained in the model parameterizations of small-scale processes. Thus the convective and large-scale transport of moist static energy is a function of the entrainment feedback, but the process of entrainment does not feature as a diabatic process in its own right, hence the potential to overlook it as a key process in the onset of organization.

Based on these findings, the hypothesis was made that progressively increasing the subgrid-scale eddy mixing strength from weak to stronger mixing should lead to the switch from random convection to an organized state, and a set of simulations using the TKE scheme confirmed this. With O(2 km) grid-sizes, updraft properties are homogeneous and the role of the mixing in organization could be exaggerated by the turbulence schemes. Clearly, simulations of RCE with higher sub-100 m grid-size will be required to test the

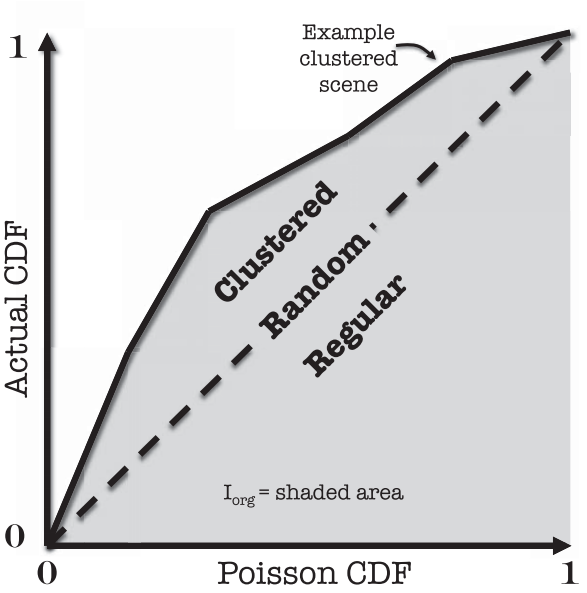


Figure 18. Schematic of organizational index (I_{org}) derivation from the model simulated NNCDF. The simulated normalized NNCDF (*y* axis) is plotted against the Poisson normalized NNCDF that would be obtained from a random distribution (*x* axis). I_{org} is the integral under the curve. A perfectly random distribution of convection would lie on the diagonal dashed line and would have $I_{org} = 0.5$. The graph shows a clustered example, for which $I_{org} > 0.5$, while a regular distribution would lie below the diagonal as annotated. Note that for a given scene, the joint NNCDF can (and often does, e.g., Figure 6a) cross the diagonal, indicating both regular and clustered organization occurring at different spatial scales.

robustness of the organizational mechanisms simulated with 2 km grid-size models, resolutions advocated previously by *Bryan et al*. [2003] and *Wyngaard* [2004]. *Sullivan and Patton* [2011] discusses resolution requirements and states that convergence is achieved when the most energetic eddies are well resolved, which is not the case at 2 km, and *Craig and Dörnbrack* [2008] also suggest that resolving clouds requires grid sizes that resolve the typical buoyancy scale of a few hundred meters. The present state of the art of LES is represented by *Heinze et al*. [2016], integrating a model for the whole of Germany with a 100 m grid spacing, for a period of 4 days.

The simulations in this paper also highlight the fact that intricacies of the assumptions contained in the parameterization of small-scale physics can strongly impact the possibility of crossing the threshold from unorganized to organized equilibrium states. The expense of such simulations has usually meant that only one model configuration is used concerning assumptions of small-scale processes such as mixing and microphysics, often initialized from a single initial condition. The potential of multiple equilibria and also an hysteresis in the transition between organized and unorganized states [*Muller and Held*, 2012], points to the requirement for larger integration ensembles employing a range of initial and boundary conditions, and physical parameterization assumptions. The ongoing requirements of large-domain, RCE numerical experiments imply that this challenge can be best met with a community-based, convective organization model intercomparison project (CORGMIP). The envisaged CORGMIP experiment would define a set of simulations protocols to allow organizational feedbacks to be diagnosed and compared with increased confidence.

Appendix A: Organization Index

It is useful to introduce a metric of convective clustering [e.g., *Tobin et al*., 2012]. Many metrics based on OLR or water vapor gauge *relative* clustering and scenes over different surface temperature boundary conditions are difficult to compare. Here a simple organization index (I_{org}) is introduced that permits one to classify a field as regular, random or clustered.

To calculate the index, updraft grid cells are identified based on a threshold vertical velocity of 1 m s^{-1} at the level of 730 hPa (2680 m) [e.g., *LeMone and Zipser*, 1980; *Robe and Emanuel*, 1996; *Tompkins*, 2000]. The domain is recursively traced to identify adjacent updraft cells as a single updraft core entity (Figure 17). For each updraft core, the distance from its geometrical centroid to that of its nearest neighbor is calculated, accounting for the periodic boundary conditions. Updraft cores cover a small fraction of the domain [*Craig*, 1996; *Tompkins and Craig*, 1998a] and thus the impact of edge effects and merging are minimized [*Weger et al*., 1992]. The cumulative density function of these nearest neighbor distances is calculated (NNCDF).

If convection were randomly organized, and thus can be considered as a Poisson point process, the expected distribution for the NNCDF is given by a Weibull distribution [*Stoyan et al*., 1987; *Weger et al*., 1992]:

$$NNCDF_{ran} = 1 - \exp(-\lambda \pi r^2). \quad \text{(A1)}$$

Here λ is the number of points per unit area (a normalizing factor) and r is the nearest neighbor distance. The NNCDF of the model simulation is compared to this theoretical random distribution (Figure 18). If the simulated distribution of convection is random at all spatial scales, then the graph of simulated versus theoretical NNCDF will lie on the diagonal. For clustered (regular) convection, the number of cores within a certain distance will exceed (be less than) that predicted by equation (A1) and the line will lie above (below) the diagonal. If information concerning the value of r is added to the graph, then it can show how clustering/regularity changes as a function of spatial scale. Various previous applications of this approach include *Weger et al*. [1992], *Benner and Curry* [1998], *Craig and Cohen* [2006], and *Seifert and Heus* [2013].

A simple index of organization (I_{org}) can be derived by integrating the area under the NNCDF graph. Random convection will have $I_{org} = 0.5$, and clustered (regular) states will have values that exceed (are less than) this. Hypothesis testing can be performed on a time series of I_{org} to determine the classification of organization. Although for a point process the index can theoretical take values ranges from zero to one, the finite grid size implies that the extreme values cannot be obtained. As the index is an integrated quantity, it is noted that a value $I_{org} = 0.5$ does not imply that convection is exactly randomly distributed at all spatial scales; it could be a result of cancellation, and the full NNCDF graph should be examined to determine how clustering changes as a function of scale.

Acknowledgments
Both authors would like to sincerely thank Greg Thompson of NCAR-RAL for extensive discussions and advice concerning the implementation and impacts of many of the parameterization scheme choices in WRF. The article was also greatly improved by two thorough anonymous reviewers. The second author was supported by a fellowship jointly awarded by ICTP (TRIL) and the International Science Programme of Uppsala University, Sweden. All model outputs used in this paper are freely available at https://doi.org/10.1594/PANGAEA.874255 in netcdf format.

References

Arakawa, A., and W. H. Shubert (1974), Interaction of a cumulus ensemble with the large- scale environment: Part 1, *J. Atmos. Sci.*, *31*, 674–701.

Benner, T. C., and J. A. Curry (1998), Characteristics of small tropical cumulus clouds and their impact on the environment, *J. Geophys. Res.*, *103*, 28,753–28,767.

Bretherton, C. S., and P. K. Smolarkiewicz (1989), Gravity waves, compensating subsidence and detrainment around cumulus clouds, *J. Atmos. Sci.*, *46*, 740–759.

Bretherton, C. S., and M. F. Khairoutdinov (2015), Convective self-aggregation feedbacks in near-global cloud-resolving simulations of an aquaplanet, *J. Adv. Model. Earth Syst.*, *7*, 1765–1787, doi:10.1002/2015MS000499.

Bretherton, C. S., M. E. Peters, and L. E. Back (2004), Relationships between water vapor path and precipitation over the tropical oceans, *J. Clim.*, *17*(7), 1517–1528.

Bretherton, C. S., P. N. Blossey, and M. Khairoutdinov (2005), An energy-balance analysis of deep convective self-aggregation above uniform SST, *J. Atmos. Sci.*, *62*, 4273–4292.

Bryan, G. H. (2005), Spurious convective organization in simulated squall lines owing to moist absolutely unstable layers, *Mon. Weather Rev.*, *133*, 1978–1997.

Bryan, G. H., J. C. Wyngaard, and J. M. Fritsch (2003), Resolution requirements for the simulation of deep moist convection, *Mon. Weather Rev.*, *131*, 2394–2416.

Coppin, D., and S. Bony (2015), Physical mechanisms controlling the initiation of convective self-aggregation in a general circulation model, *J. Adv. Model. Earth Syst.*, *7*, 2060–2078, doi:10.1002/2015MS000571.

Couhert, A., T. Schneider, J. Li, D. E. Waliser, and A. M. Tompkins (2010), The maintenance of the relative humidity in the subtropical free-troposphere, *J. Clim.*, *23*, 390–403.

Craig, G. C. (1996), Dimensional analysis of a convecting atmosphere in equilibrium with external forcing, *Q. J. R. Meteorol. Soc.*, *122*, 1963–1967.

Craig, G. C., and B. G. Cohen (2006), Fluctuations in an equilibrium convective ensemble: Part I: Theoretical formulation, *J. Atmos. Sci.*, *63*(8), 1996–2004.

Craig, G. C., and A. Dörnbrack (2008), Entrainment in cumulus clouds: What resolution is cloud-resolving?, *J. Atmos. Sci.*, *65*(12), 3978–3988.

Craig, G. C., and J. M. Mack (2013), A coarsening model for self-organization of tropical convection, *J. Geophys. Res.*, *118*, 8761–8769, doi: 10.1002/jgrd.50674.

Cronin, T. W., and K. A. Emanuel (2013), The climate time scale in the approach to radiative-convective equilibrium, *J. Adv. Model. Earth Syst.*, *5*, 843–849, doi:10.1002/jame.20049.

Dawe, J. T., and P. H. Austin (2013), Direct entrainment and detrainment rate distributions of individual shallow cumulus clouds in an LES, *Atmos. Chem. Phys.*, *13*(15), 7795–7811.

De Rooy, W. C., P. Bechtold, K. Fröhlich, C. Hohenegger, H. Jonker, D. Mironov, A. Pier Siebesma, J. Teixeira, and J.-I. Yano (2013), Entrainment and detrainment in cumulus convection: An overview, *Q. J. R. Meteorol. Soc.*, *139*(670), 1–19.

Derbyshire, S. H., I. Beau, P. Bechtold, J.-Y. Grandpeix, J.-M. Piriou, J.-L. Redelsperger, and P. M. M. Soares (2004), Sensitivity of moist convection to environmental humidity, *Q. J. R. Meteorol. Soc.*, *130*, 3055–3079.

Emanuel, K. A. (1991), A scheme for representing cumulus convection in large-scale models, *J. Atmos. Sci.*, *48*, 2313–2335.

Emanuel, K. A. (1995), The behavior of a simple hurricane model using a convective scheme based on subcloud-layer entropy equilibrium, *J. Atmos. Sci.*, *52*, 3960–3968.

Emanuel, K. A., and M. Zivkovic-Rothman (1999), Development and evaluation of a convective scheme for use in climate models, *J. Atmos. Sci.*, *56*, 1766–1782.

Emanuel, K. A., A. A. Wing, and E. M. Vincent (2014), Radiative-convective instability, *J. Adv. Model. Earth Syst.*, *6*, 75–90, doi:10.1002/2013MS000270.

Grabowski, W. W., and M. W. Moncrieff (2004), Moisture-convection feedback in the Tropics, *Q. J. R. Meteorol. Soc.*, *130*, 3081–3104.

Gray, W. M., and R. W. Jacobson Jr. (1977), Diurnal-variation of deep cumulus convection, *Mon. Weather Rev.*, *105*, 1171–1188.

Hanley, K. E., R. S. Plant, T. H. Stein, R. J. Hogan, J. C. Nicol, H. W. Lean, C. Halliwell, and P. A. Clark (2015), Mixing-length controls on high-resolution simulations of convective storms, *Q. J. R. Meteorol. Soc.*, *141*(686), 272–284.

Heinze, R., et al. (2016), Large-eddy simulations over Germany using icon: A comprehensive evaluation, *Q. J. R. Meteorol. Soc.*, *143*, 69–100, doi:10.1002/qj.2947.
Held, I. M., R. S. Hemler, and V. Ramaswamy (1993), Radiative-convective equilibrium with explicit two-dimensional moist convection, *J. Atmos. Sci.*, *50*, 3909–3927.
Holloway, C., and S. Woolnough (2016), The sensitivity of convective aggregation to diabatic processes in idealized radiative-convective equilibrium simulations, *J. Adv. Model. Earth Syst.*, *8*, 166–195, doi:10.1002/2015MS000511.
Holloway, C. E., and J. D. Neelin (2009), Moisture vertical structure, column water vapor, and tropical deep convection, *J. Atmos. Sci.*, *66*(6), 1665–1683.
Holloway, C. E., and J. D. Neelin (2010), Temporal relations of column water vapor and tropical precipitation, *J. Atmos. Sci.*, *67*(4), 1091–1105.
Hong, S. Y., Y. Noh, and J. Dudhia (2006), A new vertical diffusion package with an explicit treatment of entrainment processes, *Mon. Weather Rev.*, *134*, 2318–2341.
Hu, X.-M., J. W. Nielsen-Gammon, and F. Zhang (2010), Evaluation of three planetary boundary layer schemes in the WRF model, *J. Appl. Meteorol. Clim.*, *49*(9), 1831–1844.
Johnson, R. H., and X. Lin (1997), Episodic trade wind regimes over the western pacific warm pool, *J. Atmos. Sci.*, *54*(15), 2020–2034.
Johnson, R. H., T. M. Rickenbach, S. A. Rutledge, P. E. Ciesielski, and W. H. Shubert (1999), Trimodal characteristics of tropical convection, *J. Clim.*, *12*, 2397–2418.
Jordan, C. L. (1958), Mean soundings for the West Indies area, *J. Meteorol.*, *15*, 91–97.
Khairoutdinov, M. F., S. K. Krueger, C.-H. Moeng, P. A. Bogenschutz, and D. A. Randall (2009), Large-eddy simulation of maritime deep tropical convection, *J. Adv. Model. Earth Syst.*, *1*, *15*, doi:10.3894/JAMES.2009.1.15.
Knievel, J. C., G. H. Bryan, and J. P. Hacker (2007), Explicit numerical diffusion in the WRF Model, *Mon. Weather Rev.*, *135*, 3808–3824.
LeMone, M. A., and E. J. Zipser (1980), Cumulonimbus vertical velocity events in GATE. Part I: Diameter, intensity and mass flux, *J. Atmos. Sci.*, *37*, 2444–2457.
Lin, Y. L., R. D. Farley, and H. D. Orville (1983), Bulk parameterization of the snow field in a cloud model, *J. Clim. Appl. Meteorol.*, *22*, 1065–1092.
Machado, L. A., and J.-P. Chaboureau (2015), Effect of turbulence parameterization on assessment of cloud organization, *Mon. Weather Review*, *143*(8), 3246–3262.
Mapes, B. (2016), Gregarious convection and radiative feedbacks in idealized worlds, *J. Adv. Model. Earth Syst.*, *8*, 1029–1033, doi:10.1002/2016MS000651.
Mapes, B. E., and P. Zuidema (1996), Radiative-dynamical consequences of dry tongues in the tropical troposphere, *J. Atmos. Sci.*, *53*, 620–638.
Mauritsen, T., and B. Stevens (2015), Missing iris effect as a possible cause of muted hydrological change and high climate sensitivity in models, *Nat. Geosci.*, *8*(5), 346–351.
Mlawer, E. J., and S. Clough (1997), Shortwave and longwave enhancements in the Rapid Radiative Transfer Model, in *Proceedings of the 7th Atmospheric Radiation Measurement (ARM) Science Team Meeting*, *CONF-970365*, pp. 409–413, ARM, U.S. Dep. of Energy, Washington, D. C. [Available at http://www.arm.gov/publications.]
Mlawer, E. J., S. J. Taubman, P. D. Brown, M. J. Iacono, and S. A. Clough (1997), Radiative transfer for inhomogeneous atmospheres: RRTM, a validated correlated-k model for the longwave, *J. Geophys. Res.*, *102*, 16,663–16,682.
Muller, C. J., and I. M. Held (2012), Detailed investigation of the self-aggregation of convection in cloud-resolving simulations, *J. Atmos. Sci.*, *69*(8), 2551–2565.
Paluch, I. R. (1979), The entrainment mechanism in Colorado Cumuli, *J. Atmos. Sci.*, *36*, 2467–2478.
Pauluis, O., and S. Garner (2006), Sensitivity of radiative-convective equilibrium simulations to horizontal resolution, *J. Atmos. Sci.*, *63*(7), 1910–1923.
Pierrehumbert, R. T., and H. Yang (1993), Global chaotic mixing on isentropic surfaces, *J. Atmos. Sci.*, *50*, 2462–2480.
Polvani, L. M., and A. H. Sobel (2002), The Hadley circulation and the weak temperature gradient approximation, *J. Atmos. Sci.*, *59*(10), 1744–1752.
Popke, D., B. Stevens, and A. Voigt (2013), Climate and climate change in a radiative-convective equilibrium version of ECHAM6, *J. Adv. Model. Earth Syst.*, *5*, 1–14, doi:10.1029/2012MS000191.
Randall, D. A., and G. J. Huffman (1980), A stochastic model of cumulus clumping, *J. Atmos. Sci.*, *37*, 2068–2078.
Randall, D. A., D. A. Harshvardhan, D. A. Dazlich, and T. G. Corsetti (1989), Interactions among radiation, convection, and large-scale dynamics in a general-circulation model, *J. Atmos. Sci.*, *46*, 1943–1970.
Raymond, D. J. (1995), Regulation of moist convection over the west Pacific warm pool, *J. Atmos. Sci.*, *52*, 3945–3959.
Reed, K. A., B. Medeiros, J. T. Bacmeister, and P. H. Lauritzen (2015), Global radiative–convective equilibrium in the community atmosphere model, version 5, *J. Atmos. Sci.*, *72*(5), 2183–2197.
Robe, F. R., and K. A. Emanuel (1996), Dependence of tropical convection on radiative forcing, *J. Atmos. Sci.*, *53*, 3265–3275.
Roca, R., J. P. Lafore, C. Piriou, and J. L. Redelsperger (2005), Extratropical dry-air intrusions into the West African monsoon midtroposphere: An important factor for the convective activity over the Sahel, *J. Atmos. Sci.*, *62*, 390–407.
Romps, D. M. (2010), A direct measure of entrainment, *J. Atmos. Sci.*, *67*(6), 1908–1927.
Romps, D. M. (2016), The stochastic parcel model: A deterministic parameterization of stochastically entraining convection, *J. Adv. Model. Earth Syst.*, *8*, 319–344, doi:10.1002/2015MS000537.
Romps, D. M., and Z. Kuang (2010), Do undiluted convective plumes exist in the upper tropical troposphere?, *J. Atmos. Sci.*, *67*(2), 468–484.
Ross, A. N., A. M. Tompkins, and D. J. Parker (2004), The role of cold pools in triggering convection—A simple model, *J. Atmos. Sci.*, *61*, 1582–1595.
Rotunno, R., and K. A. Emanuel (1987), An air-sea interaction theory for tropical cyclones: Part II, *J. Atmos. Sci.*, *44*, 542–561.
Seifert, A., and T. Heus (2013), Large-eddy simulation of organized precipitating trade wind cumulus clouds, *Atmos. Chem. Phys.*, *13*, 5631–5645.
Sessions, S. L., S. Sentic, and M. J. Herman (2016), The role of radiation in organizing convection in weak temperature gradient simulations, *J. Adv. Model. Earth Syst.*, *8*, 244–271, doi:10.1002/2015MS000587.
Sherwood, S. C. (1999), Convective precursors and predictability in the tropical western Pacific, *Mon. Weather Rev.*, *127*, 2977–2991.
Sherwood, S. C., R. Roca, T. M. Weckwerth, and N. G. Andronova (2010), Tropospheric water vapor, convection, and climate, *Rev. Geophys.*, *48*, RG2001, doi:10.1029/2009RG000301.
Sherwood, S. C., D. Hernández-Deckers, M. Colin, and F. Robinson (2013), Slippery thermals and the cumulus entrainment paradox, *J. Atmos. Sci.*, *70*(8), 2426–2442.

Skamarock, W. C., J. B. Klemp, J. Dudhia, D. O. Gill, D. M. Barker, M. G. Duda, X.-Y. Huang, W. Wang, and J. G. Powers (2008), A description of the advanced research WRF Version 3, *Tech. Rep. NCAR/TN-475+STR*, Natl. Cent. Atmos. Res., Boulder, Colo. [Available at http://www2.mmm.ucar.edu/wrf/users/docs/arw_v3.pdf.]

Slingo, A., and J. M. Slingo (1988), The response of a general-circulation model to cloud longwave radiative forcing: 1: Introduction and initial experiments, *Q. J. R. Meteorol. Soc.*, *114*, 1027–1062.

Smagorinsky, J. (1963), General circulation experiments with the primative equations: I: The basic experiment, *Mon. Weather Rev.*, *91*, 99–164.

Sobel, A. H., J. Nilsson, and L. M. Polvani (2001), The weak temperature gradient approximation and balanced tropical moisture waves, *J. Atmos. Sci.*, *58*(23), 3650–3665.

Stephens, G. L., S. Van Den Heever, and L. Pakula (2008), Radiative-convective feedbacks in idealized states of radiative-convective equilibrium, *J. Atmos. Sci.*, *65*(12), 3899–3916.

Stoyan, D., W. S. Kendalla, and J. Mecke (1987), *Stochastic Geometry and Its Applications*, 345 pp., John Wiley, New York.

Stull, R. B. (1988), *An Introduction to Boundary Layer Meteorology*, 666 pp., Kluwer Acad., Dordrecht, Netherlands.

Sullivan, P. P., and E. G. Patton (2011), The effect of mesh resolution on convective boundary layer statistics and structures generated by large-eddy simulation, *J. Atmos. Sci.*, *68*(10), 2395–2415.

Takemi, T., and R. Rotunno (2003), The effects of subgrid model mixing and numerical filtering in simulations of mesoscale cloud systems, *Mon. Weather Rev.*, *131*, 2085–2101.

Tiedtke, M. (1989), A comprehensive mass flux scheme for cumulus parameterization in large-scale models, *Mon. Weather Rev.*, *117*, 1779–1800.

Tobin, I., S. Bony, and R. Roca (2012), Observational evidence for relationships between the degree of aggregation of deep convection, water vapor, surface fluxes, and radiation, *J. Clim.*, *25*(20), 6885–6904.

Tompkins, A. M. (2000), The impact of dimensionality on long-term cloud resolving model simulations, *Mon. Weather Rev.*, *128*, 1521–1535.

Tompkins, A. M. (2001a), Organization of tropical convection in low vertical wind shears: The role of water vapor, *J. Atmos. Sci.*, *58*, 529–545.

Tompkins, A. M. (2001b), On the relationship between tropical convection and sea surface temperature, *J. Clim.*, *14*, 633–637.

Tompkins, A. M. (2001c), Organization of tropical convection in low vertical wind shears: The role of coldpools, *J. Atmos. Sci.*, *58*, 1650–1672.

Tompkins, A. M., and G. C. Craig (1998a), Radiative-convective equilibrium in a three-dimensional cloud ensemble model, *Q. J. R. Meteorol. Soc.*, *124*, 2073–2097.

Tompkins, A. M., and G. C. Craig (1998b), Time-scales of adjustment to radiative-convective equilibrium in the tropical atmosphere, *Q. J. R. Meteorol. Soc.*, *124*, 2693–2713.

Tompkins, A. M., and K. A. Emanuel (2000), The vertical resolution sensitivity of simulated equilibrium temperature and water vapour profiles, *Q. J. R. Meteorol. Soc.*, *126*, 1219–1238.

Trenberth, K. E., Z. Yongxin, F. T. John, and T. Shoichi (2015), Climate variability and relationships between top of atmosphere radiation and temperatures on earth, *J. Geophys. Res.*, *120*, 3642–3659, doi:10.1002/2014JD022887.

Warner, J. (1955), The water content of cumuliform cloud, *Tellus*, *7*, 449–457.

Warner, J., and T. D. Newnham (1952), new method of measurement of cloud water content, *Q. J. R. Meteorol. Soc.*, *78*, 46–52.

Waugh, D. W., and L. M. Polvani (2000), Climatology of intrusions into the tropical upper troposphere, *Geophys. Res. Lett.*, *27*, 3857–3860.

Weger, R. C., J. Lee, T. Zhu, and R. M. Welch (1992), Clustering, randomness and regularity in cloud fields: 1: Theoretical considerations, *J. Geophys. Res.*, *97*, 20,519–20,536.

Wing, A. A., and T. W. Cronin (2016), Self-aggregation of convection in long channel geometry, *Q. J. R. Meteorol. Soc.*, *142*(694), 1–15, doi:10.1002/qj.2628.

Wing, A. A., and K. A. Emanuel (2013), Physical mechanisms controlling self aggregation of convection in idealized numerical modeling simulations, *J. Adv. Model. Earth Syst.*, *6*, 59–74, doi:10.1002/2013MS000269.

Wyngaard, J. C. (2004), Toward numerical modeling in the terra incognita, *J. Atmos. Sci.*, *61*(14), 1816–1826.

Xue, M. (1999), High-order monotonic numerical diffusion and smoothing, *Mon. Weather Rev.*, *128*, 2853–2864.

Yang, H., and R. T. Pierrehumbert (1994), Production of dry air by isentropic mixing, *J. Atmos. Sci.*, *51*, 3437–3454.

Yeo, K., and D. M. Romps (2013), Measurement of convective entrainment using Lagrangian particles, *J. Atmos. Sci.*, *70*(1), 266–277.

Zhang, C. (2005), Madden-Julian oscillation, *Rev. Geophys.*, *43*, RG2003, doi:10.1029/2004RG000158.

Zhang, C., B. E. Mapes, and B. J. Soden (2003), Bimodality in tropical water vapour, *Q. J. R. Meteorol. Soc.*, *129*(594), 2847–2866.